

RU97-10-B

# Physical Properties of the Double Exchange and Its Relevance to the Specific Heat of Double Perovskite Materials

H. C. Ren

Department of Physics, The Rockefeller University, New York,  
NY 10021, USA

M. K. Wu

Department of Physics, National Tsing Hua University, Hsinchu,  
Taiwan, ROC

## Abstract

In response to the experimental discovery of double perovskite Ru- base material, The magnetic and electronic properties of the double exchange mechanism are studied theoretically. The electron band structure and the spin wave spectrum response at zero temperature with the canting background are computed from the first principle Hamiltonian. The long range Coulomb interaction between charge carriers is found to be crucial in stabilizing the canting order. A Monte Carlo simulation is performed on de-Gennes's effective magnetic Hamiltonian with classical spin approximation. The peaks of the specific heat as a function of temperature, which correspond to FM(AF) and canting transitions, and its response to the external magnetic field are consistent with the observation. For certain region of parameters, a more complex canting order than layer type is found at sufficiently low temperature. The effective interaction between carriers via exchanging a magnon wave is found to be rather similar to that via exchanging an acoustic phonon. The pros and cons to a genuine superconducting order in this system is analyzed.

## 1. Introduction

Recently, a new type of materials of double perovskite structure is synthesized by [1], which displays a number of interesting physics [1-2]. The

molecular formula are  $Sr_2YRu_{1-x}Cu_xO_6$ ,  $Ba_2YRu_{1-x}Cu_xO_6$ , etc.. The magnetic properties are unusual with two phase transitions as a function of temperature. The underlying mechanism was conjectured to be the double exchange effect [3-5], the same mechanism partially responsible to the colossal magnetoresistance in the single perovskite compound,  $La_{2-x}Ca_xMnO_4$  [6]. In addition, the materials become superconducting for  $x \geq 0.04$  and its transition temperature reaches  $T_C = 20 - 30K$  for  $x = 0.1$ . The coherence length is about  $\xi = 35\text{\AA}$  and the super phase possess several novel features different from cuprates.

The double perovskite crystal structure of the parent compound  $(Sr, Ba)_2YRuO_6$  can be approximated by a cubic structure with the side length of a fundamental cube  $l \sim 8.16\text{\AA}$ . The  $(Ru, Cu)$  ions are located at the face-center sites, the  $Y$  ions are sitting at the octahedral sites and  $Sr$  ions at tetrahedral sites. The  $O$  ions are placed at the middle of the shortest  $Y - Ru$  bond. A small fraction of  $Ru$  is replaced by  $Cu$  through doping.

The charge balance of the ions  $Sr(Ba)$ ,  $Y$ ,  $Ru$  and  $O$  of the parent compound are +2, +3, +5 and -2. Except  $Ru^{+5}$ , the outer electronic configurations of all other ions are closed shells of the continuous rotation group. The configuration of  $Ru^{+5}$  is  $4d^3$ . It is likely that the strong Hund's rule coupling enforces the spins of the three  $d$  electrons parallel with total spin  $S = 3/2$  and their orbital wave function fill up a multiplet of the  $T_2$  representation of the cubic group, supported by  $xy$ ,  $yz$  and  $zx$  (notably, the lobes of these wave functions point to the directions of the twelve nearest neighbors of a face center site). With only the nearest neighbor antiferromagnetic exchange, the Neel state may assume a layer structure [7] perpendicular to one of the 4-fold axis with the spins of  $Ru^{+5}$  alternating along successive layers. This is consistent with the tetragonal symmetry observed by X-ray diffraction data [1]. Replacing part of  $Ru$  ions offset the charge balance and creates itinerant holes with density  $2x$  per molecule of  $(Sr, Ba)_2YRu_{1-x}Cu_xO_6$ . This may also break the symmetry further to an orthohmobic structure as indicated by the X-ray data of the doped compounds.

With itinerant holes, the state of a  $Ru$  ion is a superposition of states with charge +5, as in the parent compound and states of charge +6. In the latter case, Hund's implies a total spin  $S = 1$ . Regarding the latter states as combinations of the product states of an ion core  $Ru^{+5}$  of spin  $S = \frac{3}{2}$  and a hole of spin  $\frac{1}{2}$ . Hund's rule will prefer antiparallel spins of the ion core and the hole. The Hamiltonian combining both the antiferromagnetic exchange and the double exchange reads

$$H = \sum_{ij} J_{ij} \vec{S}_i \cdot \vec{S}_j - \frac{1}{2} \sum_{ij} t_{ij} (\Psi_i^\dagger \Psi_j + \Psi_j^\dagger \Psi_i) + \frac{1}{2} \lambda \sum_j \vec{S}_j \Psi_j^\dagger \vec{\sigma} \Psi_j + U_{Coul.}, \quad (1.1)$$

where  $\vec{S}_j$  is the total spin operator of the ion core,  $\Psi_j$ ,  $\Psi_j^\dagger$  are the creation and the annihilation operators of the itinerant holes, each of two components with spin up and spin down,  $J_{ij}$  denotes the antiferromagnetic exchange,  $t_{ij}$  denotes the hopping amplitude of the itinerant electrons and  $\lambda$  denotes the exchange interaction of the itinerant electrons with the ion cores. The Coulomb interaction,  $U_{Coul.}$ , of (1.1) is given by

$$U_{Coul.} = \frac{e^2}{8\pi\varepsilon} \left( U \sum_{j,\sigma,\sigma'} : \Psi_{j\sigma}^\dagger \Psi_{j\sigma} \Psi_{j\sigma'}^\dagger \Psi_{j\sigma'} : + \sum_{i \neq j, \sigma, \sigma'} \frac{:\Psi_{i\sigma}^\dagger \Psi_{i\sigma} \Psi_{j\sigma'}^\dagger \Psi_{j\sigma'}:}{|\vec{R}_i - \vec{R}_j|} \right), \quad (1.2)$$

where the first term represents the on-site Coulomb repulsion,  $\varepsilon$  denotes the dielectric constant of the ion cores and  $:(...):$  enforce the normal ordering. As we shall see, the long range Coulomb interaction is rather important to maintain a homogeneous canting magnetic order against clustering. The magnetic anisotropicity, the possible Jahn-Teller effect due to the degeneracy of  $d$ -band, as well as the impurity effect, which might be relevant in real systems, have been neglected for simplicity.

It was pointed out by Anderson and Hasegawa [4] that the double exchange energy, stemming from intra-atomic Hund's rule coupling, ought to be much stronger than the hopping energy, i.e.,  $\lambda S \gg t$ . In these circumstance, the effective magnetic Hamiltonian after integrating out the electronic degrees of freedom can be approximated by [6]

$$H_{\text{eff.}} = \sum_{ij} J_{ij} \vec{S}_i \cdot \vec{S}_j - \sum_{ij} b_{ij} \cos \frac{\Theta_{ij}}{2} \quad (1.3)$$

with

$$\cos \frac{\Theta_{ij}}{2} = \sqrt{\frac{1}{2} + \frac{\vec{S}_i \cdot \vec{S}_j}{2S^2}} \quad (1.4)$$

for low carrier densities

This paper addresses mainly the theoretical issues of the magnetic properties associated with the double exchange effect. Throughout this paper, we shall adopt tetragonal order for the magnetic states, which preserves the maximum subgroup symmetry of the original cubic group. Only  $J_{ij}$ 's and  $t_{ij}$ 's for nearest neighboring bond are kept different from zero for simplicity and we introduce the notations that

$$J_{ij} = \begin{cases} J, & \text{for interlayer bond } \langle ij \rangle; \\ J', & \text{for intralayer bond } \langle ij \rangle \end{cases} \quad (1.5)$$

and

$$t_{ij} = \begin{cases} t & \text{for interlayer bond } \langle ij \rangle; \\ t', & \text{for intralayer bond } \langle ij \rangle \end{cases} \quad (1.6)$$

Accordingly, the parameters  $b_{ij}$  for the effective magnetic Hamiltonian (1.3) read

$$b_{ij} = \begin{cases} b & \text{for interlayer bond } \langle ij \rangle; \\ b', & \text{for intralayer bond } \langle ij \rangle \end{cases} \quad (1.7)$$

On a cubic lattice of  $\mathcal{N}$  sites with a periodic boundary condition, there are  $2\mathcal{N}$  intra-layer bonds and  $4\mathcal{N}$  interlayer bond. Following de Gennes [5], we a homogeneous spin orientation in each layer and a canting order between successive layers. The canting angle as follows the minimization of (1.3) is

$$\cos \frac{\Theta}{2} = \frac{b}{4JS^2}. \quad (1.8)$$

This paper is organized as follows. In the section 2, we shall expand the Hamiltonian (1.1) around a canting order and examine the band structure of the itinerant holes. The first principle calculation of the magnon spectrum at zero temperature will be displayed in the section 3. The Monte Carlo simulation of the magnetic Hamiltonian (1.3) at arbitrary temperatures is presented in the section 4. The section 5 is devoted to a sketch of possible coupling between the magnon and a superconducting order. In the section 5, we shall come back to the real systems and discuss the possibility of a genuine superconducting order in them.

## 2. Mean-Field Expansion of the Hamiltonian around Canting

Denote the side length of a basic cube by  $l$  and the cubic axes, (100), (010) and (001) by  $\hat{x}, \hat{y}, \hat{z}$ . The locations magnetic ions are given by

$$\vec{R} = n_1 \vec{e}_1 + n_2 \vec{e}_2 + n_3 \vec{e}_3, \quad (2.1)$$

where  $n_1, n_2$  and  $n_3$  are integers,

$$\vec{e}_1 = \frac{l}{2}(\hat{y} + \hat{z}), \quad (2.2)$$

$$\vec{e}_2 = \frac{l}{2}(\hat{z} + \hat{x}), \quad (2.3)$$

$$\vec{e}_3 = \frac{l}{2}(\hat{x} + \hat{y}), \quad (2.4)$$

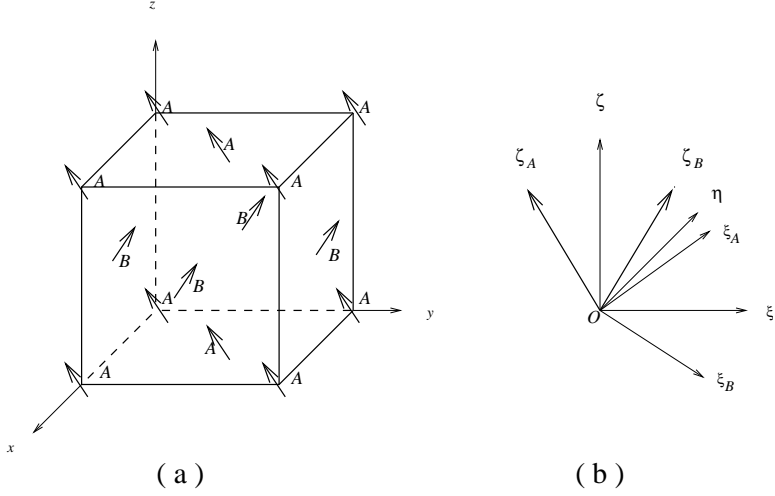


Figure 1 (a) The magnetic ordering. The magnetic sites of the sublattices  $A$  and  $B$  are marked explicitly. (b) The spin frame. The angle between  $\zeta_A$  and  $\zeta_B$  axes is  $\Theta$ .

and the total number of sites is  $\mathcal{N}$ . Adapting the tetragonal layer magnetic ordering, we divide the lattice into two sublattices shown in Fig 1. with  $n_1 + n_2 = \text{even}$  on the sublattice  $A$  and  $n_1 + n_2 = \text{odd}$  on the sublattice  $B$ . The expectation value of the ion spins of the sublattice  $A$  is denoted by  $\vec{S}_A = S\zeta_A$  and that of the sublattice  $B$  by  $\vec{S}_B = S\zeta_B$ . We choose the  $\zeta$ -axis along the direction of  $\vec{S}_A + \vec{S}_B$  and the  $\eta$ -axis as

$$\hat{\eta} = \frac{\vec{\zeta}_A \times \vec{\zeta}_B}{\sin \Theta} \quad (2.5)$$

with  $\Theta$  the mutual angle between  $\vec{S}_A$  and  $\vec{S}_B$ . We introduce further

$$\hat{\xi} = \hat{\eta} \times \hat{\zeta}, \quad (2.6)$$

$$\hat{\xi}_A = \hat{\eta} \times \hat{\zeta}_A \quad (2.7)$$

and

$$\hat{\xi}_B = \hat{\eta} \times \hat{\zeta}_B. \quad (2.8)$$

The sets  $(\hat{\xi}, \hat{\eta}, \hat{\zeta})$ ,  $(\hat{\xi}_A, \hat{\eta}, \hat{\zeta}_A)$  and  $(\hat{\xi}_B, \hat{\eta}, \hat{\zeta}_B)$  each forms a right hand coordinate system. The first of them will be referred to as the spin frame. Since the magnetic anisotropic energy has been neglected, the orientation of the spin frames does not couple with the crystal axis. The relevance of the magnetic anisotropy will be discussed in the Appendix A.

With large spin approximation [8], we write

$$\vec{S}_j = \sqrt{\frac{S}{2}}(c_j + c_j^\dagger)\hat{\xi}_A - i\sqrt{\frac{S}{2}}(c_j - c_j^\dagger)\hat{\eta} + (S - c_j^\dagger c_j)\hat{\zeta}_A + \dots \quad (2.9)$$

for the site  $j$  on the sublattice  $A$  and

$$\vec{S}_j = \sqrt{\frac{S}{2}}(d_j + d_j^\dagger)\hat{\xi}_B - i\sqrt{\frac{S}{2}}(d_j - d_j^\dagger)\hat{\eta} + (S - d_j^\dagger d_j)\hat{\zeta}_B + \dots \quad (2.10)$$

for the site  $j$  on the sublattice  $B$ , where  $c_j$ ,  $c_j^\dagger$ ,  $d_j$  and  $d_j^\dagger$  satisfy the commutation relations of elementary boson operators. After some algebra, which is shown in detail in Appendix B, the Hamiltonian (1.1) is expanded as

$$H = H_0 + H_1 + H_2 + H_3 + H_4, \quad (2.11)$$

where

$$H_0 = 2\mathcal{N}S^2(J' + 2J\cos\Theta), \quad (2.12)$$

$$H_1 = 4JS^{\frac{3}{2}}\sqrt{2\mathcal{N}}(\zeta_0 + \zeta_0^\dagger)\sin\Theta, \quad (2.13)$$

$$\begin{aligned} H_2 = & \sum_{\vec{p}} \psi_{\vec{p}}^\dagger(E'_{\vec{p}} - \mu)\psi_{\vec{p}} + \sum_{\vec{p}} (\nu_{\vec{p}}^+ \zeta_{\vec{p}}^\dagger \zeta_{\vec{p}} + \nu_{\vec{p}}^- z_{\vec{p}}^\dagger z_{\vec{p}}) \\ & - JS \sin^2 \frac{\Theta}{2} \sum_{\vec{p}} v_{\vec{p}}(z_{\vec{p}} z_{-\vec{p}} + z_{-\vec{p}}^\dagger z_{\vec{p}}^\dagger - \zeta_{\vec{p}} \zeta_{-\vec{p}} - \zeta_{-\vec{p}}^\dagger \zeta_{\vec{p}}^\dagger) \end{aligned} \quad (2.14)$$

$$\text{with } \nu_{\vec{p}}^\pm = 2S \left[ J'(-2 + u_{\vec{p}}) - 4J\cos\Theta \mp Jv_{\vec{p}} \cos^2 \frac{\Theta}{2} \right],$$

$$\begin{aligned} H_3 = & -\lambda \sqrt{\frac{S}{2\mathcal{N}}} \sum_{\vec{p}, \vec{q}} \left[ \zeta_{\vec{q}} \psi_{\vec{p} + \frac{\vec{q}}{2}}^\dagger \tau_- \psi_{\vec{p} - \frac{\vec{q}}{2}} + \zeta_{\vec{q}}^\dagger \psi_{\vec{p} - \frac{\vec{q}}{2}}^\dagger \tau_+ \psi_{\vec{p} + \frac{\vec{q}}{2}} \right. \\ & \left. + z_{\vec{q}} \psi_{\vec{p} + \frac{\vec{q}}{2}}^\dagger \rho_1 \tau_- \psi_{\vec{p} - \frac{\vec{q}}{2}} + z_{\vec{q}}^\dagger \psi_{\vec{p} - \frac{\vec{q}}{2}}^\dagger \rho_1 \tau_+ \psi_{\vec{p} + \frac{\vec{q}}{2}} \right] + \text{three-magnon terms}, \end{aligned} \quad (2.15)$$

$$\begin{aligned} H_4 = & -\frac{\lambda}{2\mathcal{N}} \sum_{\vec{p}, \vec{p}', \vec{q}} \left[ (\zeta_{\vec{p}' - \frac{\vec{q}}{2}}^\dagger \zeta_{\vec{p}' + \frac{\vec{q}}{2}} + z_{\vec{p}' - \frac{\vec{q}}{2}}^\dagger z_{\vec{p}' + \frac{\vec{q}}{2}}) \psi_{\vec{p}' + \frac{\vec{q}}{2}}^\dagger \tau_3 \psi_{\vec{p}' - \frac{\vec{q}}{2}} \right. \\ & \left. + (\zeta_{\vec{p}' - \frac{\vec{q}}{2}}^\dagger z_{\vec{p}' + \frac{\vec{q}}{2}} + z_{\vec{p}' - \frac{\vec{q}}{2}}^\dagger \zeta_{\vec{p}' + \frac{\vec{q}}{2}}) \psi_{\vec{p}' + \frac{\vec{q}}{2}}^\dagger \rho_1 \tau_3 \psi_{\vec{p}' - \frac{\vec{q}}{2}} \right] + \text{four-magnon terms} \end{aligned} \quad (2.16)$$

and

$$\begin{aligned} U_{Coul.} = & \frac{e^2}{\mathcal{N}\varepsilon} \sum_{\vec{p}, \vec{p}', \vec{q}} \left( D_{\vec{q}}^{(0)} \psi_{\vec{p} + \frac{\vec{q}}{2}}^\dagger \psi_{\vec{p}' - \frac{\vec{q}}{2}}^\dagger \psi_{\vec{p}' + \frac{\vec{q}}{2}} \psi_{\vec{p} - \frac{\vec{q}}{2}} \right. \\ & \left. + D_{\vec{q}}^{(0)\prime} (\rho_1)_{\alpha\beta} (\rho_1)_{\alpha'\beta'} \psi_{\vec{p} + \frac{\vec{q}}{2}\alpha}^\dagger \psi_{\vec{p}' - \frac{\vec{q}}{2}\alpha'}^\dagger \psi_{\vec{p}' + \frac{\vec{q}}{2}\beta'} \psi_{\vec{p} - \frac{\vec{q}}{2}\beta} \right). \end{aligned} \quad (2.17)$$

In (2.15)-(2.16), only the terms we shall use are exhibited explicitly. The magnon operators  $\zeta_{\vec{p}}$  and  $z_{\vec{p}}$  of (2.13)-(2.16) are related to  $c_j$  and  $d_j$  via

(B.1), (B.2), (B.19) and (B.20) in the appendix. The hole operator  $\psi_{\vec{p}}$  of (2.14)-(2.17) is a  $4 \times 1$  column matrix and is related to the  $2 \times 1$  column matrix  $\Psi_j$  through (B.3), (B.4) and (B.21). The  $4 \times 4$  Dirac matrices

$$\tau_1 = \begin{pmatrix} \sigma_1 & 0 \\ 0 & \sigma_1 \end{pmatrix}, \tau_2 = \begin{pmatrix} \sigma_2 & 0 \\ 0 & \sigma_2 \end{pmatrix}, \tau_3 = \begin{pmatrix} \sigma_3 & 0 \\ 0 & \sigma_3 \end{pmatrix} \quad (2.18)$$

and

$$\rho_1 = \begin{pmatrix} 0 & I \\ I & 0 \end{pmatrix}, \rho_2 = \begin{pmatrix} 0 & -iI \\ iI & 0 \end{pmatrix}, \rho_3 = \begin{pmatrix} I & 0 \\ 0 & -I \end{pmatrix} \quad (2.19)$$

with

$$[\rho_a, \tau_b] = 0 \quad (2.20)$$

and

$$\tau_{\pm} = \frac{1}{2}(\tau_1 \pm i\tau_2) \quad (2.21)$$

have been introduced accordingly, where  $I$  is a  $2 \times 2$  unit matrix and  $\sigma_a$ 's are Pauli matrices. The Bloch momentum  $\vec{p}(\vec{p}', \vec{q})$  throughout (2.13-17) corresponds to the translational invariance within each sublattice. In terms of the dimensionless parameters

$$\alpha_1 = \frac{l}{2}(p_x + p_y), \quad (2.22)$$

$$\alpha_2 = \frac{l}{2}(-p_x + p_y) \quad (2.23)$$

and

$$\alpha_3 = p_z l, \quad (2.24)$$

the Brillouin zone is specified as  $\pi < \alpha_1, \alpha_2, \alpha_3 \leq \pi$ , the function  $u_{\vec{p}}$  and  $v_{\vec{p}}$  of (2.14) is given by

$$u_{\vec{p}} = \cos \alpha_1 + \cos \alpha_2 \quad (2.25)$$

and

$$v_{\vec{p}} = 4 \cos \frac{\alpha_1}{2} \cos \frac{\alpha_2}{2} \cos \frac{\alpha_3}{2}, \quad (2.26)$$

and the bare Coulomb propagators  $D_{\vec{q}}^{(0)}$  and  $D_{\vec{q}}^{(0)\prime}$  of (2.17) read

$$D_{\vec{q}}^{(0)} = \frac{4}{l(2\alpha_{\perp}^2 + \alpha_3^2)} + U - \frac{0.36485}{l} \quad (2.27)$$

and

$$D_{\vec{q}}^{(0)\prime} = U - \frac{0.17943}{l}. \quad (2.28)$$

The Hamiltonian (2.11)-(2.17) is invariant under the tetragonal crystal rotation, inversion, and the  $\mathcal{C}$ -transformation introduced in the appendix B,

$$\mathcal{C}z_{\vec{p}}\mathcal{C}^{-1} = -z_{\vec{p}} \quad (2.29)$$

$$\mathcal{C}\zeta_{\vec{p}}\mathcal{C}^{-1} = \zeta_{\vec{p}} \quad (2.30)$$

and

$$\mathcal{C}\psi_{\vec{p}}\mathcal{C}^{-1} = -\rho_3\psi_{\vec{p}}. \quad (2.31)$$

The matrix of the hole kinetic energy  $E_{\vec{p}}$  is given by

$$E_{\vec{p}} - \mu = -t'u_{\vec{p}} - tv_{\vec{p}}\rho_3\left(\tau_3 \cos \frac{\Theta}{2} - \tau_1 \sin \frac{\Theta}{2}\right) + \frac{1}{2}\lambda S\tau_3 - \mu, \quad (2.32)$$

which is easily diagonalized and produces four energy bands:

$$\epsilon_{\vec{p},s}^{\pm} = -t'(u_{\vec{p}} + \mu) - s\Delta_{\vec{p}}^{\pm} \quad (2.33)$$

for  $\mathcal{C} = 1$  and

$$\epsilon_{\vec{p},s}^{-} = -t'(u_{\vec{p}} + \mu) - s\Delta_{\vec{p}}^{-} \quad (2.34)$$

for  $\mathcal{C} = -1$ , where  $s = \pm 1$  and

$$\Delta_{\vec{p}}^{\pm} = \sqrt{\frac{1}{4}\lambda^2 S^2 \pm \lambda S t v_{\vec{p}} \cos \frac{\Theta}{2} + t^2 v_{\vec{p}}^2}. \quad (2.35)$$

The wave functions corresponding to the four bands are

$$\mathcal{U}_{\vec{p},s}^{\pm} = \begin{pmatrix} \phi_{\vec{p},s}^{\pm} \\ 0 \end{pmatrix} \quad (2.36)$$

for  $\epsilon_{\vec{p},s}^{\pm}$  and

$$\mathcal{U}_{\vec{p},s}^{-} = \begin{pmatrix} 0 \\ \phi_{\vec{p},s}^{-} \end{pmatrix} \quad (2.37)$$

for  $\epsilon_{\vec{p},s}^{-}$ , where  $2 \times 1$  matrices  $\phi_{\vec{p},s}^{\pm}$  are defined by

$$\frac{1}{\Delta_{\vec{p}}^{\pm}} \left[ \left( \frac{1}{2}\lambda S \pm t v_{\vec{p}} \cos \frac{\Theta}{2} \right) \sigma_3 \mp t v_{\vec{p}} \sigma_1 \sin \frac{\Theta}{2} \right] \phi_{\vec{p},s}^{\pm} = s \phi_{\vec{p},s}^{\pm}. \quad (2.38)$$

The electron spin ceases to be a good quantum number and the only degeneracies in Brillouin zone correspond the points related by the space inversion

and the proper tetragonal rotations. The density of states of the four bands are plotted in Fig. 2.

The free electron propagator with energy  $p_0$  and momentum  $\vec{p}$  is given by:

$$S(p_0, \vec{p}) = \int_{-\infty}^{\infty} dt e^{ip_0 t} \langle |T\psi_{\vec{p}}(t)\psi_{\vec{p}}(0)^\dagger| \rangle = S^+(p_0, \vec{p})\rho_- + S^-(p_0, \vec{p})\rho_+ \quad (2.39)$$

$$S^\pm(p_0, \vec{p}) = i \frac{p_0 + t' u_{\vec{p}} \pm t v_{\vec{p}} \tau'_3 + \frac{1}{2} \lambda S \tau_3}{(p_0 + t' u_{\vec{p}})^2 - \Delta_{\vec{p}}^{\pm 2}} \quad (2.40)$$

with

$$\tau'_3 = \tau_3 \cos \frac{\Theta}{2} - \tau_1 \sin \frac{\Theta}{2} \quad (2.41)$$

and  $T\dots$  the time ordering symbol. The state  $| \rangle$  in (2.39) denotes the Fermi sea of the itinerant holes and the time evolution of  $\psi_{\vec{p}}$  is generated by the quadratic hole Hamiltonian.

### 3. Magnetic Energies with Normal Holes

In this section we shall calculate the ground state energy and the spin wave spectrum at zero temperature using the Hamiltonian (2.11)-(2.17). For the sake of simplicity, we assume that only the band  $\epsilon_{\vec{p},+}^+$  is partially filled and denote

$$\epsilon_{\vec{p},+}^+ \equiv \epsilon_{\vec{p}} = -t' u_{\vec{p}} - \Delta_{\vec{p}} - \mu \quad (3.1)$$

with

$$\Delta_{\vec{p}} = \sqrt{\frac{1}{4} \lambda^2 S^2 + \lambda S t v_{\vec{p}} \cos \frac{\Theta}{2} + t^2 v_{\vec{p}}^2} \quad (3.2)$$

As we shall see in the next section, the incorporation of possible superconductivity orders does not modify the result drastically. We confine ourselves within the normal phase of the carriers in this section.

The basic ingredients of the Feynman diagrams are displayed in Fig. 3

A dashed line with a plus sign or minus sign represents a magnon propagator with  $\mathcal{C} = \pm 1$ , whose expression is

$$\frac{i}{q_0 - \nu_{\vec{q}}^{\pm} + i0^+} \quad (3.3)$$

for  $\mathcal{C} = \pm 1$ . A two point vertex with two incoming or two outgoing magnons is associated with  $\mp 2iJSv_{\vec{q}} \sin^2 \frac{\Theta}{2}$  for  $\mathcal{C} = \pm 1$ . A solid line represents a

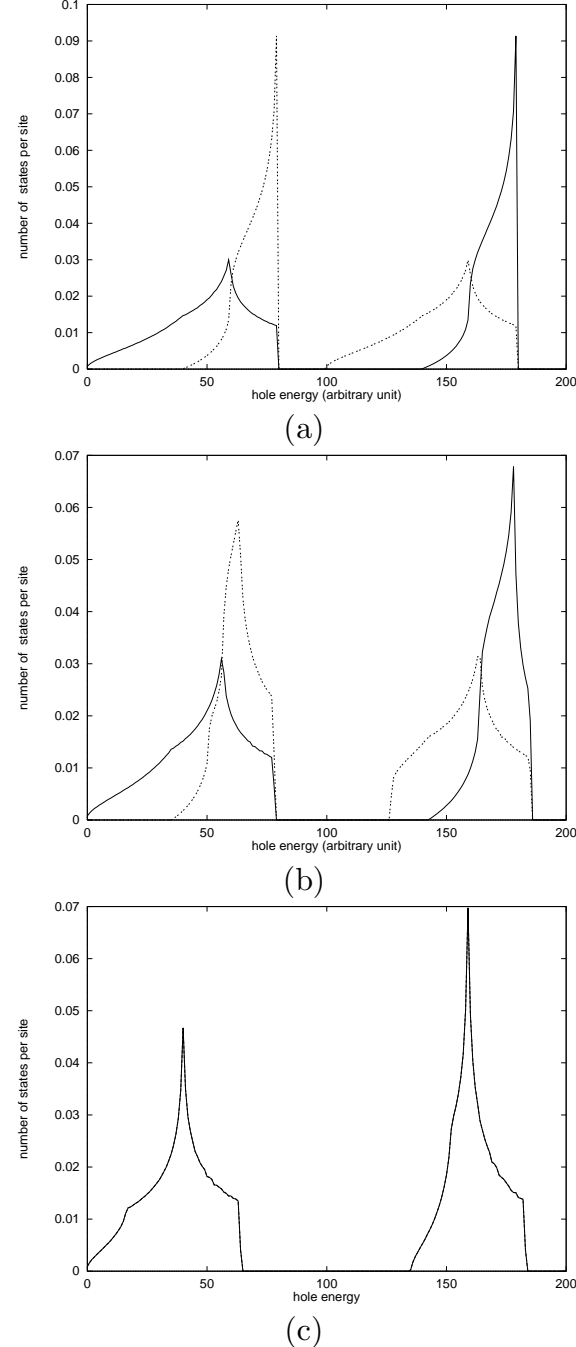


Figure 2 The density of states of itinerant holes at several canting angles. (a)  $\Theta = 0$ ; (b)  $\Theta = 90^\circ$ ; (c)  $\Theta = 180^\circ$ . The solid line represents the band with  $\mathcal{C} = 1$ . and the dashed line represents the band with  $\mathcal{C} = -1$ . Both kinds of bands degenerate for the pure antiferromagnetic order (c)

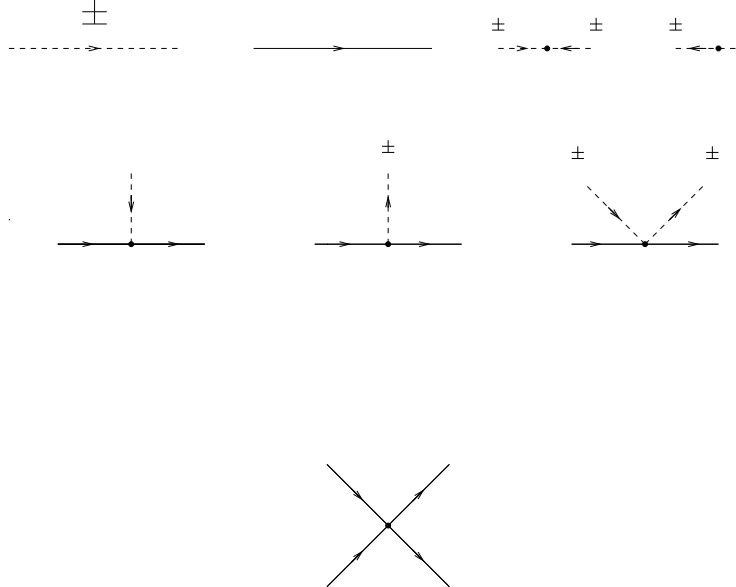


Figure 3 Some elements of the Feynman diagrams of the Hamiltonian (2.11)-(2.17).

hole propagator and is associated with the expression (2.40). A vertex with an incoming and an outgoing holes and an incoming(outgoing) magnon of  $\mathcal{C} = 1$  is associated with the factor  $i\lambda\sqrt{\frac{S}{2N}}\tau_-(\tau_+)$  and that with an incoming(outgoing) magnon of  $\mathcal{C} = -1$  with  $i\lambda\sqrt{\frac{S}{2N}}\rho_1\tau_-(\tau_+)$ . A vertex with two hole lines and two magnon lines of the same  $\mathcal{C}$  is associated with a factor  $i\frac{\lambda}{2N}\tau_3$ . A Coulomb vertex with two incoming and two outgoing electrons is associated with  $-i\frac{2}{N}(D_{\vec{q}}^{(0)} + D_{\vec{q}}^{(0)\prime}\rho_1)$  with  $\vec{q}$  the momentum being transferred in the scattering, where the exchange term has been neglected. Other vertices of (2.11)-(2.17) may also be read off easily but the above ingredients are all we need for the following calculations.

### 3.1 The ground state energy

The free energy of the ground state per site in the grand canonical ensemble comes from the magnetic terms, (2.12) and the Fermi sea and reads

$$f = 2S^2(J' + 2J\cos\Theta) + \frac{1}{N} \sum_{\vec{p}} \theta(-\epsilon_{\vec{p}})\epsilon_{\vec{p}}. \quad (3.4)$$

Diagrammatically, the Fermi sea term corresponds to  $i \times$  a closed hole loop. The canting angle is determined by the minimization condition

$$\left(\frac{\partial f}{\partial \Theta}\right)_\mu = 0, \quad (3.5)$$

and we obtain

$$\cos \frac{\Theta}{2} = \frac{\lambda t}{32JS} \sum_{\vec{p}} \frac{v_{\vec{p}}}{\Delta_{\vec{p}}} \theta(-\epsilon_{\vec{p}}). \quad (3.6)$$

Diagrammatically, this condition eliminates the sum of tadpole diagrams to the order of tree level of the magnon lines and one loop level of hole lines. The hole density  $n_h$ , the number of holes per site, is related to the chemical potential through

$$n_h = \left( \frac{\partial f}{\partial \mu} \right)_{\Theta} = \frac{1}{\mathcal{N}} \sum_{\vec{p}} \theta(-\epsilon_{\vec{p}}). \quad (3.7)$$

The solution of (3.6) and (3.7) determines the canting angle and the chemical potential as a function of the hole density. By a Legendre transformation, we obtain the canonical ground state energy

$$u = f + \mu n_h = 2(J' + 2J \cos \Theta)S^2 + \frac{1}{\mathcal{N}} \sum_{\vec{p}} \theta(-\epsilon_{\vec{p}})(\epsilon_{\vec{p}} + \mu), \quad (3.8)$$

in which the chemical potential and the canting angle are expressed in terms of  $n_h$  with the aid of (3.6) and (3.7). With a strong double exchange,  $\lambda S \gg t, t'$ ,

$$\epsilon_{\vec{p}} = -\frac{1}{2}\lambda S - t'u_{\vec{p}} - tv_{\vec{p}} \cos \frac{\Theta}{2} - \mu \quad (3.9)$$

and the sum over  $\vec{p}$  is restricted near the bottom of the band at low hole densities  $n_h \ll 1$ , and an explicit expression of  $\Theta$  follows from (3.6), i.e.

$$\cos \frac{\Theta}{2} = \frac{n_h t}{4JS^2}. \quad (3.10)$$

This can be reconciled with the formula (1.8) by setting  $b = n_h t$ . Substituting this into (3.8) we find

$$u = 2(J' - 2J)S^2 - \left( \frac{1}{2}\lambda S + 2t' \right) n_h - \frac{t^2}{2JS^2} n_h^2. \quad (3.11)$$

The expression of (3.10) and (3.11) was also obtained by de Gennes [5] with the magnetic Hamiltonian (1.3).

### 3.2 The magnon spectrum

Following the standard strategy, we introduce two self energy functions  $\Pi_{\pm}(q_0, \vec{q})$  and  $\Lambda_{\pm}(q_0, \vec{q})$ , where  $\Pi_{\pm}(q_0, \vec{q})$  represents the sum of all amputated one particle irreducible diagrams with an incoming and an outgoing magnons of  $\mathcal{C} = \pm 1$  and  $\Lambda_{\pm}(q_0, \vec{q})$  the sum of all one particle irreducible diagrams with two incoming (two outgoing) magnons of  $\mathcal{C} = \pm 1$ . Then the full propagator with an incoming and an outgoing magnons reads

$$\mathcal{D}_{\pm}(q_0, \vec{q}) = \frac{-iF_{\pm}(-q_0, -\vec{q})}{-F_{\pm}(q_0, \vec{q})F_{\pm}(-q_0, -\vec{q}) + \Lambda_{\pm}^2(q_0, \vec{q})} \quad (3.12)$$

and that with two incoming (two outgoing) magnons reads

$$\mathcal{V}_{\pm}(q_0, \vec{q}) = -i \frac{\Lambda_{\pm}(q_0, \vec{q})}{-F_{\pm}(q_0, \vec{q})F_{\pm}(-q_0, -\vec{q}) + \Lambda_{\pm}^2(q_0, \vec{q})}, \quad (3.13)$$

where

$$F_{\pm}(q_0, \vec{q}) = q_0 - \nu_{\vec{q}}^{\pm} - \Pi_{\pm}(q_0, \vec{q}). \quad (3.14)$$

The magnon spectrum is determined by the pole condition:

$$-F_{\pm}(q_0, \vec{q})F_{\pm}(-q_0, -\vec{q}) + \Lambda_{\pm}^2(q_0, \vec{q}) = 0. \quad (3.15)$$

The derivation of (3.12) and (3.13) follows the same steps as for dressed propagators of an interacting boson system with a Bose condensate[9].

The self energy functions have been computed to the order of one hole loop and the relevant diagrams are exhibited in Fig. 4.

Note that the Debye screening of the long range Coulomb interaction has been included in the  $\mathcal{C} = 1$  branch since it plays a crucial rule to stabilize the canting order. The computation is straightforward and we list in the following the main results in the approximation  $\lambda S \gg t, t'$

$\mathcal{C} = 1$  Branch[10]:

$$\Pi_{+}(q_0, \vec{q}) = \Pi_{+}^{(0)}(q_0, \vec{q}) + \Pi_{+}^{(1)}(q_0, \vec{q}), \quad (3.16)$$

where  $\Pi_{+}^{(0)}(q_0, \vec{q})$  denotes (a)+(b), the part without Coulomb vertices, and is given by

$$\begin{aligned} \Pi_{+}^{(0)}(q_0, \vec{q}) &= \frac{\lambda}{2\mathcal{N}} \sum_{\vec{p}} \theta(-\epsilon_{\vec{p}}) \times \\ &\times \left[ 1 - \frac{\lambda S}{\lambda S + q_0 + t'(u_{\vec{p}} - u_{\vec{p}-\vec{q}}) + t(v_{\vec{p}} + v_{\vec{p}-\vec{q}}) \cos \frac{\Theta}{2}} \right] \end{aligned}$$

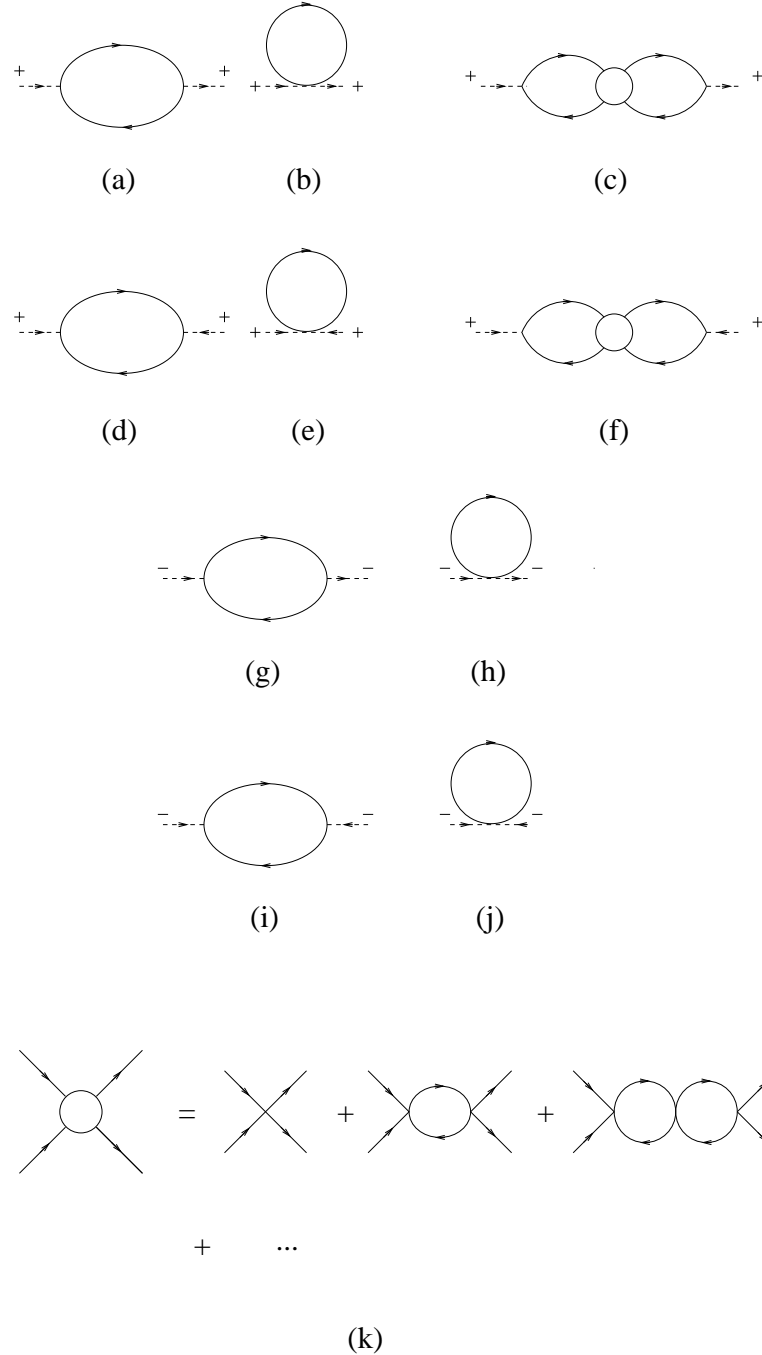


Figure 4 Feynmann diagrams for the magnon self energy functions  $\Pi_{\pm}(q_0, \vec{q})$  and  $\Lambda_{\pm}(q_0, \vec{q})$ . The trivial diagrams giving rise to the first terms of (3.22) and (3.26) are not displayed.

$$+ \frac{t^2}{2\mathcal{N}S} \sin^2 \frac{\Theta}{2} \sum_{\vec{p}} v_{\vec{p}-\frac{\vec{q}}{2}}^2 \frac{\theta(-\epsilon_{\vec{p}+\frac{\vec{q}}{2}}) - \theta(-\epsilon_{\vec{p}-\frac{\vec{q}}{2}})}{\epsilon_{\vec{p}+\frac{\vec{q}}{2}} - \epsilon_{\vec{p}-\frac{\vec{q}}{2}} - q_0} \quad (3.17)$$

and  $\Pi_+^{(1)}(q_0, \vec{q})$  comes from the screened Coulomb force,

$$\Pi_+^{(1)}(q_0, \vec{q}) = (c) = \frac{t^2}{2S} C^2(q_0, \vec{q}) D(q_0, \vec{q}) \sin^2 \frac{\Theta}{2}, \quad (3.18)$$

where  $C(q_0, \vec{q})$  corresponds to the coupling between a magnon of  $\mathcal{C} = 1$  to the density fluctuation and reads

$$C(q_0, \vec{q}) = \frac{1}{\mathcal{N}} \sum_{\vec{p}} v_{\vec{p}-\frac{\vec{q}}{2}} \frac{\theta(-\epsilon_{\vec{p}+\frac{\vec{q}}{2}}) - \theta(-\epsilon_{\vec{p}-\frac{\vec{q}}{2}})}{\epsilon_{\vec{p}+\frac{\vec{q}}{2}} - \epsilon_{\vec{p}-\frac{\vec{q}}{2}} - q_0} \quad (3.19)$$

and  $\mathcal{D}(q_0, \vec{q})$  corresponds to the dressed Coulomb propagator

$$D(q_0, \vec{q}) = (k) = \frac{e^2 D_{\vec{q}}^{(0)}}{\varepsilon + e^2 D_{\vec{q}}^{(0)} \sigma(q_0, \vec{q})} \quad (3.20)$$

with the density-density correlation function,  $\sigma(q_0, \vec{q})$ , given by

$$\sigma(q_0, \vec{q}) = -\frac{1}{\mathcal{N}} \sum_{\vec{p}} \frac{\theta(-\epsilon_{\vec{p}+\frac{\vec{q}}{2}}) - \theta(-\epsilon_{\vec{p}-\frac{\vec{q}}{2}})}{\epsilon_{\vec{p}+\frac{\vec{q}}{2}} - \epsilon_{\vec{p}-\frac{\vec{q}}{2}} - q_0}. \quad (3.21)$$

Likewise, we have

$$\Lambda_+(q_0, \vec{q}) = 2JS v_{\vec{q}} \sin^2 \frac{\Theta}{2} + \Lambda_+^{(0)}(q_0, \vec{q}) + \Lambda_+^{(1)}(q_0, \vec{q}), \quad (3.22)$$

where

$$\begin{aligned} \Lambda_+^{(0)}(q_0, \vec{q}) = (d) + (e) &= \frac{t^2}{2\mathcal{N}S} \sin^2 \frac{\Theta}{2} \sum_{\vec{p}} v_{\vec{p}+\frac{\vec{q}}{2}} v_{\vec{p}-\frac{\vec{q}}{2}} \times \\ &\times \frac{\theta(-\epsilon_{\vec{p}+\frac{\vec{q}}{2}}) - \theta(-\epsilon_{\vec{p}-\frac{\vec{q}}{2}})}{\epsilon_{\vec{p}+\frac{\vec{q}}{2}} - \epsilon_{\vec{p}-\frac{\vec{q}}{2}} - q_0} \end{aligned} \quad (3.23)$$

and

$$\Lambda_+^{(1)}(q_0, \vec{q}) = (f) = \frac{t^2}{2S} C(q_0, \vec{q}) D(q_0, \vec{q}) C(-q_0, -\vec{q}) \sin^2 \frac{\Theta}{2}. \quad (3.24)$$

$\mathcal{C} = -1$  Branch:

$$\begin{aligned} \Pi_-(q_0, \vec{q}) = & \frac{\lambda}{2\mathcal{N}} \sum_{\vec{p}} \theta(-\epsilon_{\vec{p}}) \left[ 1 - \frac{\lambda S}{\lambda S + q_0 + t'(u_{\vec{p}} - u_{\vec{p}-\vec{q}}) + t(v_{\vec{p}} - v_{\vec{p}-\vec{q}}) \cos \frac{\Theta}{2}} \right] \\ & + \frac{t^2}{2\mathcal{N}S} \sin^2 \frac{\Theta}{2} \sum_{\vec{p}} v_{\vec{p}-\frac{\vec{q}}{2}}^2 \left[ \frac{\theta(-\epsilon_{\vec{p}+\frac{\vec{q}}{2}})}{-q_0 + t'(u_{\vec{p}-\frac{\vec{q}}{2}} - u_{\vec{p}+\frac{\vec{q}}{2}}) - t(v_{\vec{p}-\frac{\vec{q}}{2}} + v_{\vec{p}+\frac{\vec{q}}{2}}) \cos \frac{\Theta}{2}} \right. \\ & \left. + \frac{\theta(-\epsilon_{\vec{p}-\frac{\vec{q}}{2}})}{q_0 + t'(u_{\vec{p}+\frac{\vec{q}}{2}} - u_{\vec{p}-\frac{\vec{q}}{2}}) - t(v_{\vec{p}+\frac{\vec{q}}{2}} + v_{\vec{p}-\frac{\vec{q}}{2}}) \cos \frac{\Theta}{2}} \right] \end{aligned} \quad (3.25)$$

and

$$\begin{aligned} \Lambda_-(q_0, \vec{q}) = & -2JSv_{\vec{q}} \sin^2 \frac{\Theta}{2} - \frac{t^2}{2\mathcal{N}S} \sin^2 \frac{\Theta}{2} \sum_{\vec{p}} v_{\vec{p}+\frac{\vec{q}}{2}} v_{\vec{p}-\frac{\vec{q}}{2}} \times \\ & \times \left[ \frac{\theta(-\epsilon_{\vec{p}+\frac{\vec{q}}{2}})}{-q_0 + t'(u_{\vec{p}-\frac{\vec{q}}{2}} - u_{\vec{p}+\frac{\vec{q}}{2}}) - t(v_{\vec{p}-\frac{\vec{q}}{2}} + v_{\vec{p}+\frac{\vec{q}}{2}}) \cos \frac{\Theta}{2}} \right. \\ & \left. + \frac{\theta(-\epsilon_{\vec{p}-\frac{\vec{q}}{2}})}{q_0 + t'(u_{\vec{p}+\frac{\vec{q}}{2}} - u_{\vec{p}-\frac{\vec{q}}{2}}) - t(v_{\vec{p}+\frac{\vec{q}}{2}} + v_{\vec{p}-\frac{\vec{q}}{2}}) \cos \frac{\Theta}{2}} \right] \end{aligned} \quad (3.26)$$

It follows from the equilibrium condition (3.6) for the canting angle that

$$F_{\pm}(0, p\hat{z}) + \Lambda_{\pm}(0, p\hat{z}) = 0. \quad (3.27)$$

The case with  $\vec{p} = 0$  of this equation is the consequence of the Goldstone theorem and (3.27) is found to hold without the large  $\lambda S$  approximation. Furthermore we find

$$F_-(0, 0) - \Lambda_-(0, 0) = 0, \quad (3.28)$$

$$\begin{aligned} F_+(0, 0) - \Lambda_+(0, 0) = & -16JS \sin^2 \frac{\Theta}{2} \\ & + \frac{1}{\mathcal{N}} \frac{t^2}{2S} \sin^2 \frac{\Theta}{2} (\langle v_{\vec{p}}^2 \rangle - \langle v_{\vec{p}} \rangle^2) \sum_{\vec{p}} \delta(-\epsilon_{\vec{p}}), \end{aligned} \quad (3.29)$$

where  $\langle \dots \rangle$  denotes the average over the Fermi surface

$$\langle F_{\vec{p}} \rangle \equiv \frac{\sum_{\vec{p}} F_{\vec{p}} \delta(-\epsilon_{\vec{p}})}{\sum_{\vec{p}} \delta(-\epsilon_{\vec{p}})}. \quad (3.30)$$

A simple expression of the magnon spectrum can be obtained at low carrier density  $n_h \ll 1$  and with a parabolic approximation of the band. The  $q_0$

dependence of  $\Pi_{\pm}(q_0, \vec{q})$  and  $\Lambda_{\pm}(q_0, \vec{q})$  may be dropped under the condition that  $q_0 \ll v_F q$  with  $v_F$  the Fermi velocity. The second term of (3.29) may also be neglected since it is smaller than the first term by a factor of the order of  $n_h^{\frac{2}{3}}$  and eq. (3.27) becomes

$$q_0^2 - [\nu_{\vec{q}}^{\pm} + \Pi_{\pm}(0, \vec{q})]^2 + \Lambda_{\pm}^2(0, \vec{q}) = 0 \quad (3.31)$$

with  $q_0$  replaced by  $\omega_{\pm}$  we obtain the following long wavelength formula for the magnon energy:

$$\omega_{+} = 4\alpha_{\perp} \sin \frac{\Theta}{2} \sqrt{JS \left[ -J'S + \frac{n_h}{4S} t' + \frac{tt' n_h \sin^2 \frac{\Theta}{2} \sec \frac{\Theta}{2}}{4S(t' + t \cos \frac{\Theta}{2})} \right]} \quad (3.32)$$

for  $\mathcal{C} = +1$  and

$$\omega_{-} = \alpha_{\perp} \sqrt{(-J'S + \frac{n_h}{4S} t' \sec^2 \frac{\Theta}{2}) \left[ (-J'S + \frac{n_h}{4S} t') \alpha_{\perp}^2 + JS \alpha^2 \sin^2 \frac{\Theta}{2} \right]} \quad (3.33)$$

for  $\mathcal{C} = -1$ .  $\alpha_{\perp}$  and  $\alpha$  of (3.32) and (3.33) are related to the cartesian components of  $\vec{q}$  through

$$\alpha_{\perp}^2 = \frac{l^2}{2} (q_x^2 + q_y^2) \quad (3.34)$$

and

$$\alpha^2 = \frac{l^2}{2} (q_x^2 + q_y^2 + 2q_z^2). \quad (3.35)$$

The expressions (3.32) and (3.33) are different, though not far, from that obtain by de Gennes using the magnetic Hamiltonian (1.3). Both branches contribute to the specific heat a power law  $T^{\frac{3}{2}}$  dependence at low  $T$ . This is different from the observed suppression of the low temperature specific heat in the doped samples. It is not likely, as we shall see in the next section that the coupling to a genuine superconducting order will improve the situation. A possible explanation is the magnetic anisotropy, which freezes the spin frame to some preferred orientation. The detail of this effect will be discussed in the Appendix A.

The approximate equation (3.31) inspires an effective Hamiltonian for low momentum magnon spectrum

$$H_{\text{mag.}} = \sum_{\vec{q}} x_{\vec{q}}^+ \zeta_{\vec{q}}^{\dagger} \zeta_{\vec{q}} + \sum'_{\vec{q}} y_{\vec{q}}^+ (\zeta_{\vec{q}} \zeta_{-\vec{q}} + \zeta_{-\vec{q}}^{\dagger} \zeta_{\vec{q}}^{\dagger})$$

and

$$+ \sum_{\vec{q}} x_{\vec{q}}^- z_{\vec{q}}^\dagger z_{\vec{q}}^- + \sum_{\vec{q}}' y_{\vec{q}}^- (z_{\vec{q}} z_{-\vec{q}} + z_{-\vec{q}}^\dagger z_{\vec{q}}^\dagger) \quad (3.36)$$

with

$$x_{\vec{q}}^\pm = \nu_{\vec{q}}^\pm + \Pi^\pm(0, \vec{q}) \quad (3.37)$$

and

$$y_{\vec{q}}^\pm = \Lambda^\pm(0, \vec{q}). \quad (3.38)$$

The magnon of  $\mathcal{C} = -1$  is stable against decay to this order and that of  $\mathcal{C} = 1$  is not. The decay width of the latter is calculated in the Appendix C and is found much smaller than the energy (3.32), for large  $S$  and small  $n_h$ .

The most remarkable lesson we learned from above Green function formalism is that the role played by the long range Coulomb interaction. If the  $\Pi_+^{(1)}(q_0, \vec{q})$  term of (3.16) were not there,  $\Pi_+(q_0, \vec{q})$  would be dominated by the second term of  $\Pi_+^{(0)}(q_0, \vec{q})$ , which is of the order  $n_h^{\frac{1}{3}}$  and is negative. This would make (3.29) positive for  $\mathcal{C} = 1$  and the corresponding solution for magnon energy imaginary. This is associated with the negative coefficient of the  $n_h^2$  term of the bulk energy (3.11), which would be unstable against clustering if the holes were electrically neutral. It is the long range Coulomb interaction that turns (3.29) negative and a real magnon spectrum follows. This effect can not be obtained from the magnetic Hamiltonian (1.3).

#### 4. Monte Carlo Simulation of the effective Magnetic Hamiltonian

The calculations of the last two sections are restricted to the zero temperature. For finite temperatures, numerical simulation is the only means of exploring the phase transitions. The Hamiltonian (1.1), involving both spin and fermion variables is prohibitively complicated to perform a Monte Carlo simulation on a sufficiently large lattice. Therefore we switch to the effective magnetic Hamiltonian (1.3) with classical spins. The argument which justify such an approximation can be found in [6].

The partition function corresponding to the Hamiltonian (1.3) is

$$Z = \int \prod_j d^2 \vec{S}_j e^{-\frac{H_{\text{eff}}}{k_B T}} \quad (4.2)$$

where we have made classical approximation of the spins and the integration  $d^2 \vec{S}_j$  is over the solid angle of  $\vec{S}_j$  with its magnitude fixed. The internal

energy per magnetic site is given by

$$u = k_B T^2 \frac{\partial}{\partial T} \ln Z \quad (4.3)$$

and the specific heat per site is given by

$$c_V = \frac{\partial u}{\partial T}. \quad (4.4)$$

The high temperature expansion of the internal energy per site,  $u$ , obtained by expanding the integrand of (5.2) to a power series of  $\frac{H_{\text{eff}}}{k_B T}$  and the first few terms give rise to

$$u = -\frac{4}{3}(b' + 2b) - \frac{2}{3} \frac{A' + 2A}{k_B T} + \frac{8}{3} \frac{B}{(k_B T)^2} + O((k_B T)^{-3}), \quad (4.5)$$

where

$$A = J^2 S^4 - \frac{4}{5} J b S^2 + \frac{1}{6} b^2, \quad (4.6)$$

$$A' = J'^2 S^4 - \frac{4}{5} J' b' S^2 + \frac{1}{6} b'^2, \quad (4.7)$$

and

$$B = (JS^2 - \frac{2}{5}b)^2 (J'S^2 - \frac{2}{5}b') + (\frac{6197}{48000} - \frac{9}{64}G)b^2 b' \quad (4.8)$$

with  $G$  the Catalan's constant given by

$$G = \sum_{n=0}^{\infty} \frac{(-1)^n}{(2n+1)^2} = 0.9160. \quad (4.9)$$

The corresponding specific heat reads

$$c_V = \left[ \frac{2}{3} \frac{A' + 2A}{(k_B T)^2} - \frac{16}{3} \frac{B}{(k_B T)^3} + O((k_B T)^{-4}) \right] k_B. \quad (4.10)$$

At low temperature, equal partition theorem implies that

$$u = u_0 + k_B T \quad (4.11)$$

and the specific heat approaches  $k_B$ . and therefore can not be trusted there.

Extensive Monte carlo simulation has been performed on this system. There are four parameters in the magnetic Hamiltonian and three dimensionless ratio can be formed:  $J'/J \leq 1$ , which measure the anisotropicity of the antiferromagnetic exchange;  $b'/b$ , which measure the anisotropicity of

the double exchange, and  $b/JS^2$ , which measure the strength of the double exchange relative to the AF exchange. All these ratios are expected to be doping dependent. It follows from the specific heat data for  $x = 0$  that  $J' \sim J$ . The specific heat data also indicate that significant anisotropy is developed with doping. Therefore, we simulated a number of  $J'/J$  ratio for  $b = b' = 0$  and only two ratios  $J'/J = -0.4, 0.5$  are considered for  $b, b' \neq 0$ . In the latter case, we are more interested in the interplay between the double exchange and AF exchange for various  $b$  and  $b'$  is chosen to equal to  $b$  for the sake of simplicity. Most of the results except the finite size scaling behavior are extracted from a lattice of 2000 sites. The heat bath algorithm was used for the simulations without double exchange and Metropolis [11] algorithm was used for the simulations with double exchange.

Fig. 5 shows the phase diagram for  $J'/J = -0.4, 0.5$ , obtained from the MC study as compared with the corresponding mean field result of de Gennes [5]. The magnitude of the transition temperature for various  $b$  is reduced from MF by about a factor 2 but the demarkation point between AF dominance and FM dominance remains close to the MF value  $b/JS^2 = 2.5$ . The specific heat extracted from long MC runs are plotted in Fig.6 for several  $b$  value at  $J'/J = -0.4$ .

The two peaks corresponds to the transitions from disordered phase to the FM(AF) phase at higher  $T$  and the transitions from FM phase to the canting phase at lower  $T$ . 24000 configurations are included in the average for the data points. The estimated error ranges from one percent outside the critical region to ten percent inside the the region. As the two transition approach each other, its always the peak at higher  $T$  that is suppressed. This is consistent with the experimental fact that the higher  $T$  peak is somehow less sharper than the other one[2]. The scaling behavior as the lattice size increases from  $\mathcal{N} = 250$  to  $\mathcal{N} = 6750$  is displayed in Fig. 7 and the growth of these peaks indicate two genuine phase transition as  $\mathcal{N} \rightarrow \infty$ .

The canting order can be viewed as a superposition of FM and AF orders. As the temperature is lowered for  $b/JS^2 < 2.5$ , the system enter this phase from AF order. In another word, a FM order is triggered at the lower transition temperature. On the other hand, as the temperature is lowered for  $b/JS^2 > 2.5$ , the system enter the canting phase from FM order and a AF order is triggered at the lower transition temperature. Since a homogeneous magnetic field couple directly to the FM order only, we expect that the peak at lower  $T$  is sensitive to the external magnetic field for  $b/JS^2 < 2.5$  and the peak at higher  $T$  is sensitive for  $b/JS^2 > 2.5$ . This is indeed the case for the MC results of the specific heat with an external magnetic field shown in Fig.8.

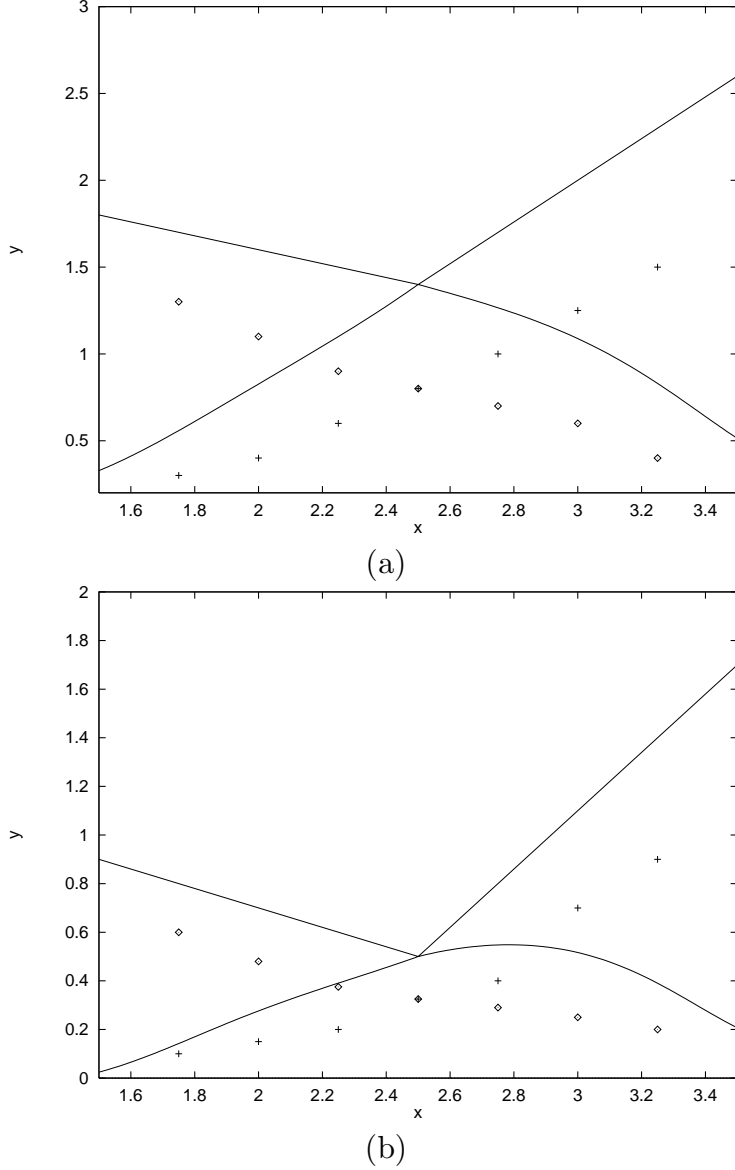


Figure 5 The Monte Carlo results of the magnetic phase diagrams for (a)  $\frac{J'}{J} = -0.4$ ; (b)  $\frac{J'}{J} = 0.5$ . The solid lines is given by the molecular field approximation [5]. The diamonds denote the onset of an antiferromagnetic order and the crosses denote the onset of a ferromagnetic order.  $x = \frac{b}{JS^2}$ ,  $y = \frac{k_B T}{5J}$  with  $k_B$  the Boltzmann constant.

## 5. Coupling to the Superconducting Order

Under the assumption that only the band with  $\mathcal{C} = 1$  and energy (3.1), referred to as the conducting band, is partially filled, the superconducting

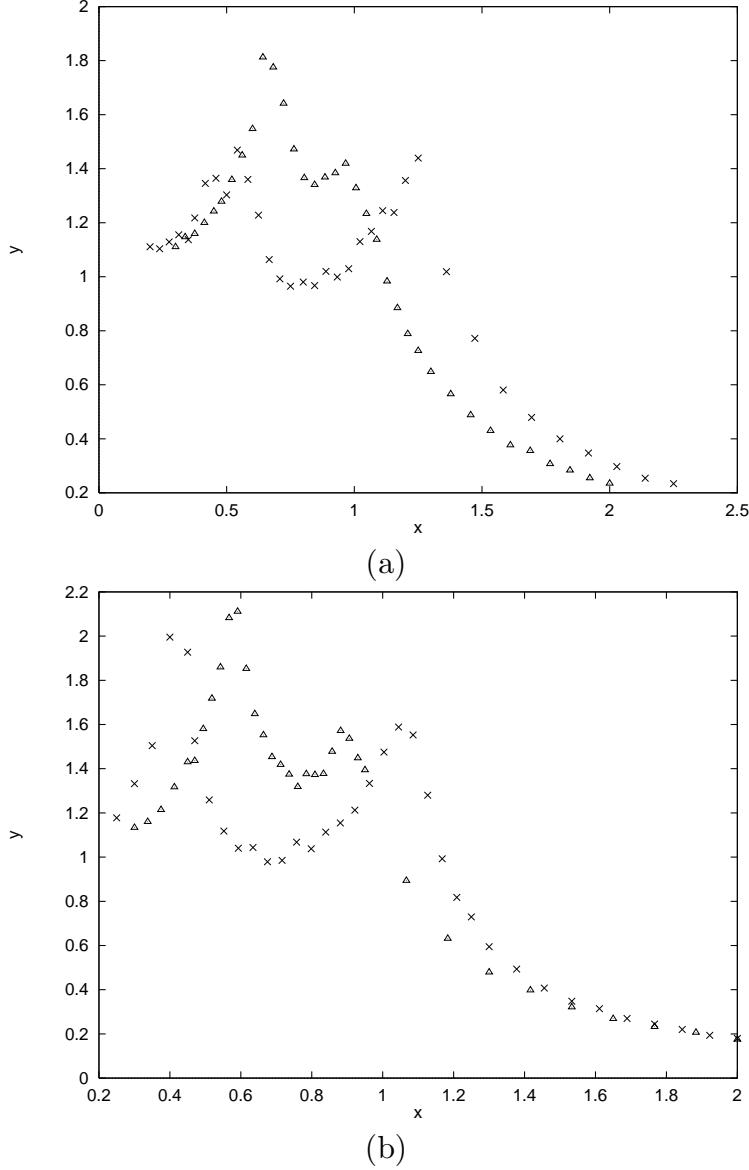


Figure 6 The Monte Carlo results for the specific heat for several strengths of the double exchange and  $\frac{J'}{J} = -0.4$ ;  $x = \frac{k_BT}{5J}$  and  $y = c_V$  in arbitrary unit. (a)  $\frac{b}{JS^2} = 3$  (cross), 2.75(triangle); (b)  $\frac{b}{JS^2} = 2$ (cross), 2.25(triangle).

pairing, if there is any, has to be of odd parity. The spin orientation of the two partners of a pairing with momenta  $\vec{p}$  and  $-\vec{p}$  are parallel, like the pairing in the  $A$  phase of  $He^3$ [12]. But, the orientation itself depends on the magnitude of  $\vec{p}$ . The collective mode (Bogoliubov mode) originated from the long range order has the  $\mathcal{C}$  number one and is liable to couple with the magnon of the same channel.

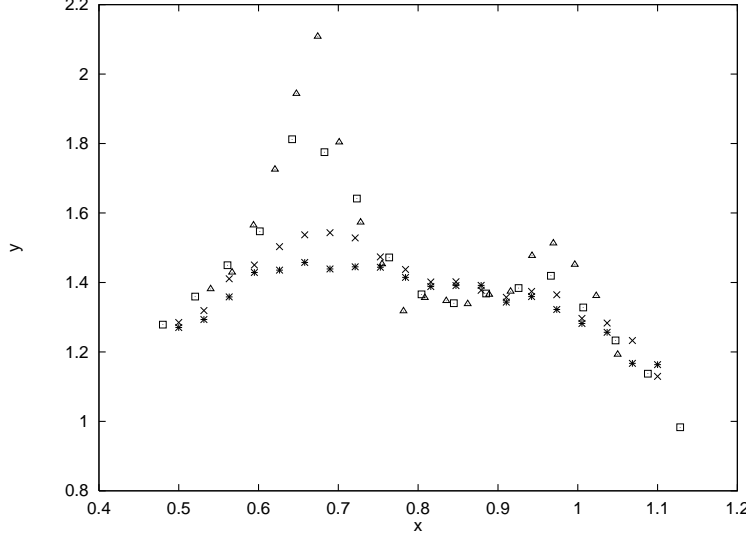


Figure 7 The scaling behavior of the specific heat for  $\mathcal{N} = 250$ (star), 432(cross), 2000(square) and 6750(triangle) near the transitions, where  $\frac{J'}{J} = -0.4$ ,  $\frac{b}{JS^2} = 2.75$ ,  $x = \frac{b}{JS^2}$  and  $y = c_V$  in arbitrary unit.

Introduce the annihilation and creation operators of the itinerant holes,  $a_{\vec{p}s}^\iota$  and  $a_{\vec{p}}^{\iota\dagger}$  with  $\iota$  and  $s$  labeling the quantum numbers of the four bands ( $\iota = \pm$  for  $\mathcal{C} = \pm 1$ ), the hole-magnon coupling term of the Hamiltonian can be written as

$$H_3 = -\sqrt{\frac{1}{\mathcal{N}}} \sum_{\vec{p}, \vec{p}', \iota, s} [\lambda_{\vec{p}, \vec{q}, s}^\iota \zeta_{\vec{q}} a_{\vec{p}'s}^{\iota\dagger} a_{\vec{p}s}^\iota + \lambda_{\vec{p}, \vec{q}, s}^{\iota*} \zeta_{\vec{q}}^\dagger a_{\vec{p}'s}^{\iota\dagger} a_{\vec{p}s}^\iota + \dots], \quad (5.1)$$

where we show explicitly only the terms preserving the  $\mathcal{C}$  number of the holes.

$$\lambda_{\vec{p}, \vec{p}'s}^\iota = \sqrt{\frac{S}{2}} \lambda \phi_{\vec{p}'s}^{\iota\dagger} \sigma - \phi_{\vec{p}s}^\iota \quad (5.2)$$

with  $\phi_{\vec{p}s}^\iota$  the  $2 \times 1$  wave function defined in (2.36). Consider the scattering process of two holes with opposite momenta

$$h(\vec{p}) + h(-\vec{p}) \rightarrow h(\vec{p}') + h(-\vec{p}')$$

with  $\vec{q} = \vec{p}' - \vec{p}$  and  $|\vec{q}| \ll |\vec{p}|$ . The second order perturbation in  $H_3$  produce an energy dependent effective potential mediating the two holes, i.e.

$$\begin{aligned} U_{\text{eff.}} = & -i \left[ \lambda_{\vec{p}', \vec{p}} \lambda_{-\vec{p}', -\vec{p}}^* [\mathcal{D}(q_0, \vec{q}) + \mathcal{V}(q_0, \vec{q})] \right. \\ & \left. - \lambda_{-\vec{p}', \vec{p}} \lambda_{\vec{p}', -\vec{p}}^* [\mathcal{D}(P_0, \vec{P}) + \mathcal{V}(P_0, \vec{P})] \right] \end{aligned} \quad (5.3)$$

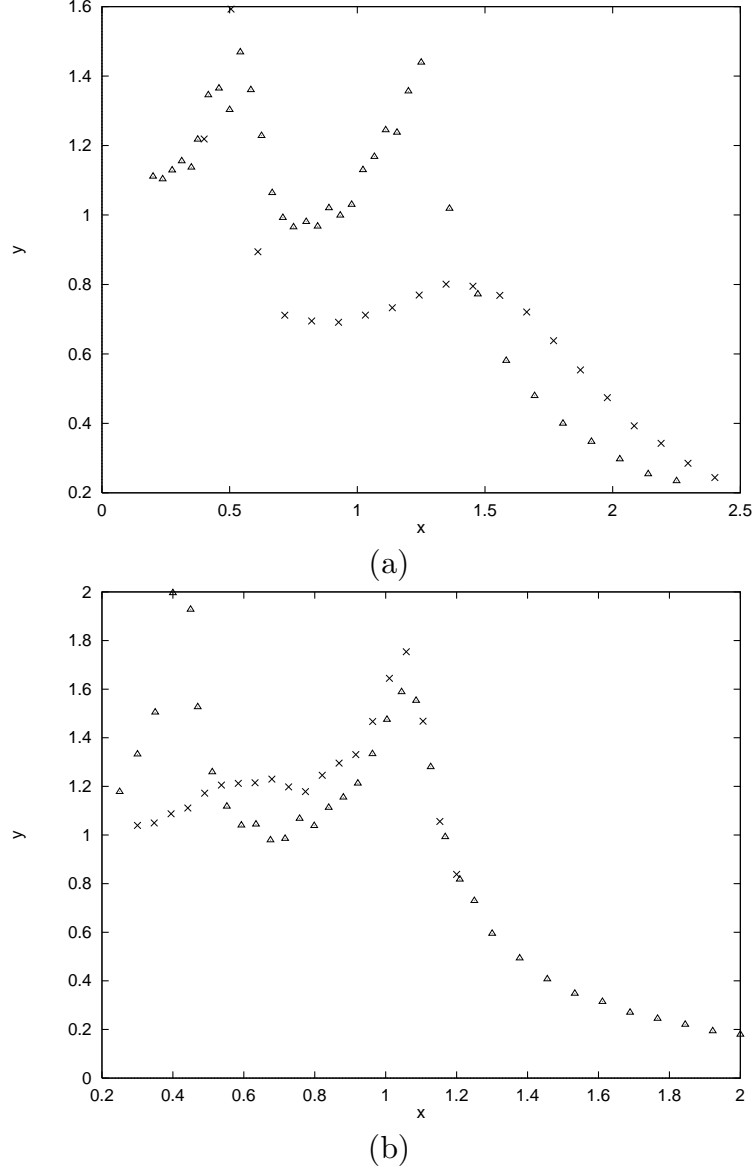


Figure 8 The effect of an external magnetic field on the specific heat peaks for  $\frac{J'}{J} = -0.4$  and  $\frac{b}{JS^2} = 3$ (a), 2(b). The triangles correspond to zero external field,  $\frac{\mu_B}{JS^2} = 0$  and the crosses to  $\frac{\mu_B}{JS^2} = 0.5$ ;  $x = \frac{k_B T}{5J}$  and  $y = c_V$  in arbitrary unit.

with  $P_0 = p_0 + p'_0$  and  $\vec{P} = \vec{p} + \vec{p}'$ , which consists of the direct interaction (the first term) and the exchange interaction (the second term). For  $\vec{p}$  and  $\vec{p}'$  near the Fermi surface and  $\vec{q} \rightarrow 0$ , the direct term dominate and we have

$$U_{\text{eff.}} = \frac{8t^2}{S} \sin^2 \frac{\Theta}{2} \frac{\frac{\omega_q^2}{16JS} \csc \frac{\Theta}{2}}{q_0^2 - \omega_q^2}, \quad (5.4)$$

where  $\omega_{\vec{q}}$  is given by (3.32) and the superscript has been suppressed and we have also substitute the approximation

$$\lambda_{\vec{p}',\vec{p},s}^{\iota} = \iota s 2 \sqrt{\frac{2}{S}} t \sin \frac{\Theta}{2}. \quad (5.5)$$

at low carrier density. The effective potential (5.4) is rather similar to the effective potential mediated by an acoustic phonon, which is retarded and attractive, and is felt by holes in all bands. The large core spin  $S$  here plays a similar role as the large ion mass for the electron(hole)-phonon coupling and we expect that the Migdal theorem [13] holds for sufficiently large  $S$ . Furthermore such an attraction would not be there for just ferromagnetic order alone,  $\Theta = 0$ , a point stressed also in [14]. There is a simple physical reason: Like the electron-phonon coupling, the effective attraction is achieved through local polarization of the ions by charge carriers, the attraction here is caused by local distortion of the ion spins. The counter reaction of this distortion would flip the carriers spin, which would cost huge amount of energy  $\sim \lambda S$  with only ferromagnetic order, since the spin orientation in the conduction band point to a unique direction. With canting order, the spin orientation in the conduction band varies with the Bloch momentum and the local ion spins can be distorted at much less cost of energy. In addition to (5.4), there may be other attractions induced by large hole-phonon coupling caused by Jahn-Taylor effect. On the other hand, we are still far from inferring that there are sufficient attractions to beat the Coulomb repulsion. Furthermore the exchange term in (5.4) has to be considered for single specie pairing.

Leaving aside the pairing mechanism, we may still study the coupling of the magnon with the superconducting order by adding a pairing term to the Haniltonian (2.11). The total Hamiltonian reads now,

$$\mathcal{H} = H + \sum_{\vec{q}} \beta_{\vec{q}}^{\dagger} \beta_{\vec{q}}, \quad (5.6)$$

where  $a_{\vec{p}}, a_{\vec{p}}^{\dagger}$  stands for the annihilation and creation operators of the itinerant holes, and  $\beta_{\vec{q}}, \beta_{\vec{q}}^{\dagger}$  stands for composite boson operators which represent Cooper pairs, i.e.,

$$\beta_{\vec{q}} = \frac{1}{\sqrt{\mathcal{N}}} \sum'_{\vec{p}} g_{\vec{p},\vec{q}} a_{\vec{p}+\frac{\vec{q}}{2}} a_{-\vec{p}+\frac{\vec{q}}{2}} \quad (5.7)$$

with  $\sum'_{\vec{p}}$  extends over half of the Brillouin zone only. The pairing wave function,  $g_{\vec{p},\vec{q}}$ , is odd under the space inversion, i.e.

$$g_{\vec{p},\vec{q}} = -g_{-\vec{p},\vec{q}} \quad (5.8)$$

on account of the anticommutation relation among  $a_{\vec{p}}$ 's [15]. The superconductivity is implemented through the condensation of the pairing operator of zero total momentum, i.e.

$$\langle S | \beta_{\vec{q}=0} | S \rangle = \sqrt{\mathcal{N}} B, \quad (5.9)$$

where  $B$  is the long range order parameter and is chosen to be real and positive for the sake of simplicity. At the presence of (5.9), the part of the total Hamiltonian (5.6), which is quadratic in  $a$  and  $a^\dagger$  reads

$$H_{SC} = \sum_{\vec{p}} \epsilon_{\vec{p}} a_{\vec{p}}^\dagger a_{\vec{p}} + \sum'_{\vec{p}} (\delta_{\vec{p}}^* a_{\vec{p}} a_{-\vec{p}} + \delta_{\vec{p}} a_{-\vec{p}}^\dagger a_{\vec{p}}^\dagger) \quad (5.10)$$

with  $\epsilon_{\vec{p}}$  given by (3.1) and

$$\delta_{\vec{p}} = B g_{\vec{p}, \vec{q}}|_{\vec{q}=0} = |\delta_{\vec{p}}| e^{i\gamma_{\vec{p}}}. \quad (5.11)$$

$H_{SC}$  can be diagonalized by the Bogoliubov transformation

$$\begin{aligned} a_{\vec{p}} &= \alpha_{\vec{p}} \cos \theta_{\vec{p}} - e^{i\gamma_{\vec{p}}} \alpha_{-\vec{p}}^\dagger \sin \theta_{\vec{p}} \\ a_{-\vec{p}}^\dagger &= e^{-i\gamma_{\vec{p}}} \alpha_{\vec{p}} \sin \theta_{\vec{p}} + \alpha_{-\vec{p}}^\dagger \cos \theta_{\vec{p}}, \end{aligned} \quad (5.12)$$

where

$$\begin{aligned} \cos 2\theta_{\vec{p}} &= \frac{\epsilon_{\vec{p}}}{\mathcal{E}_{\vec{p}}} \\ \sin 2\theta_{\vec{p}} &= \frac{|\delta_{\vec{p}}|}{\mathcal{E}_{\vec{p}}} \end{aligned} \quad (5.13)$$

with  $\mathcal{E}_{\vec{p}} = \sqrt{\epsilon_{\vec{p}}^2 + |\delta_{\vec{p}}|^2}$ . and we have

$$H_{SC} = \frac{1}{2} \sum_{\vec{p}} (\epsilon_{\vec{p}} - \mathcal{E}_{\vec{p}}) + \sum_{\vec{p}} \mathcal{E}_{\vec{p}} \alpha_{\vec{p}}^\dagger \alpha_{\vec{p}}. \quad (5.14)$$

The free energy density of the ground state, (3.4), is replaced by

$$f = 2S^2 (J' + 2J \cos \Theta) + \frac{1}{\mathcal{N}} \frac{1}{2} \sum_{\vec{p}} (\epsilon_{\vec{p}} - \mathcal{E}_{\vec{p}}). \quad (5.15)$$

The canting angle is determined now by

$$\cos \frac{\Theta}{2} = \frac{\lambda t}{32JS} \sum_{\vec{p}} \frac{v_{\vec{p}}}{\Delta_{\vec{p}}} \frac{\mathcal{E}_{\vec{p}} - \epsilon_{\vec{p}}}{2\mathcal{E}_{\vec{p}}}, \quad (5.16)$$

and the expression of the carrier density (3.7) becomes

$$n_h == \frac{1}{\mathcal{N}} \sum_{\vec{p}} \frac{\mathcal{E}_{\vec{p}} - \epsilon_{\vec{p}}}{2\mathcal{E}_{\vec{p}}}. \quad (5.17)$$

In addition to the strong double exchange and low carrier density, we assume that the gap energy comparable or smaller than the Fermi energy. It follows then that the expression (3.10) for  $\Theta$  remains an approximate solution of (5.16) and (5.17). The reason is that the canting is induced by the delocalization of the charge carriers, which lower the energy of the kinetic energy by an amount of the order hopping amplitude, while the approximation amounts to assume that other energy scales (Fermi energy and gap energy) are much smaller than that.

The superconducting order affect the magnon spectrum in two ways. The first of them amounts to dress the hole lines in Fig. 4 with the long range order. On writing the  $\mathcal{C} = 1$  branch of the hole propagator,  $S^+(p_0, \vec{p})$  of (2.40) as

$$S^+(p_0, \vec{p}) = i \left( \frac{Z_{\vec{p}}^+}{p_0 - \epsilon_{\vec{p}}} + \frac{Z_{\vec{p}}^-}{p_0 - \epsilon_{\vec{p}} + 2\Delta_{\vec{p}}} \right), \quad (5.18)$$

where  $Z_{\vec{p}}^\pm$  are  $2 \times 2$  matrices

$$Z_{\vec{p}}^\pm = \phi_{\vec{p}\pm}^+ \phi_{\vec{p}\pm}^{+\dagger} = \frac{1}{2} \left( 1 \mp \frac{tv_{\vec{p}}\sigma'_3 + \frac{1}{2}\lambda S\sigma_3}{\Delta_{\vec{p}}} \right). \quad (5.19)$$

Only the first term is subject to the modification. The factor

$$\frac{i}{p_0 - \epsilon_{\vec{p}}} = \int_{-\infty}^{\infty} dt e^{ip_0 t} \langle |T a_{\vec{p}}(t) a_{\vec{p}}(0)^\dagger| \rangle \quad (5.20)$$

of (5.18) ought to be replaced by

$$\int_{-\infty}^{\infty} dt e^{ip_0 t} \langle S | T a_{\vec{p}}(t) a_{\vec{p}}(0)^\dagger | S \rangle = \frac{i(p_0 + \epsilon_{\vec{p}})}{p_0^2 - \mathcal{E}_{\vec{p}}^2}, \quad (5.21)$$

where  $|S\rangle$  denotes the ground state with the long range order, (5.9), and the time evolution of  $a_{\vec{p}}(t)$  is governed by the Hamiltonian (5.14). Anomalous propagators

$$\int_{-\infty}^{\infty} dt e^{ip_0 t} \langle S | T a_{\vec{p}}(t) a_{-\vec{p}}(0) | S \rangle = \frac{i\delta_{\vec{p}}}{p_0^2 - \mathcal{E}_{\vec{p}}^2} \quad (5.22)$$

and

$$\int_{-\infty}^{\infty} dt e^{ip_0 t} \langle S | T a_{-\vec{p}}(t)^\dagger a_{-\vec{p}}(0)^\dagger | S \rangle = \frac{i\delta_{\vec{p}}^*}{p_0^2 - \mathcal{E}_{\vec{p}}^2} \quad (5.23)$$

should also be included. The hole propagator of the  $\mathcal{C} = -1$  channel  $S^-(p_0, \vec{p})$ , however, remains unchanged. With these modifications, the same magnon spectrum (3.32) and (3.33) emerge as the leading order of the approximation stated following (5.17).

The second type of influence of the superconducting order is the mixing of the magnon of  $\mathcal{C} = 1$  and the collective (Bogoliubov mode). Instead of an extensive diagrammatic analysis, we take a short cut. We first calculate the amplitude of the following two processes:

$$\text{I: } |i\rangle = \zeta_{\vec{q}}^\dagger |S\rangle, |f\rangle = \beta_{\vec{q}}^\dagger |S\rangle;$$

$$\text{II: } |i\rangle = \zeta_{\vec{q}}^\dagger \beta_{-\vec{q}}^\dagger |S\rangle, |f\rangle = |S\rangle$$

where,  $|i\rangle$  and  $|f\rangle$  denote the initial and final states. Using (4.1), (4.7), we find that

$$\kappa \equiv \lim_{\vec{q} \rightarrow 0} \langle f | H_3 | i \rangle = \frac{tB}{4\mathcal{N}\sqrt{S}} \sin \frac{\Theta}{2} \sum_{\vec{p}} |g_{\vec{p},0}|^2 \frac{\mathcal{E}_{\vec{p}} + \epsilon_{\vec{p}}}{\mathcal{E}_{\vec{p}}^2}. \quad (5.24)$$

From now on, we regard  $\beta_{\vec{q}}$  and  $\beta_{\vec{q}}^\dagger$  as elementary boson operators and introduce the following effective Hamiltonian for the mixing

$$\begin{aligned} H_{\text{eff.}} = & \sum_{\vec{p}} x_{\vec{p}} \zeta_{\vec{p}}^\dagger \zeta_{\vec{p}} + \sum_{\vec{p}}' y_{\vec{p}} (\zeta_{\vec{p}} \zeta_{-\vec{p}} + \zeta_{-\vec{p}}^\dagger \zeta_{\vec{p}}^\dagger) \\ & + \sum_{\vec{p}} \xi_{\vec{p}} \beta_{\vec{p}}^\dagger \beta_{\vec{p}} + \sum_{\vec{p}}' \eta_{\vec{p}} (\beta_{\vec{p}} \beta_{-\vec{p}} + \beta_{-\vec{p}}^\dagger \beta_{\vec{p}}^\dagger) \\ & + \kappa \sum_{\vec{p}} (\beta_{\vec{p}}^\dagger \zeta_{\vec{p}} + \beta_{\vec{p}} \zeta_{-\vec{p}} + \text{h.c.}), \end{aligned} \quad (5.25)$$

where  $x_{\vec{p}}$  and  $y_{\vec{p}}$  here are the same as  $x_{\vec{p}}^+$  and  $y_{\vec{p}}^+$  in (3.38) and (3.39) and the structure bosonic part Hamiltonian can be obtained simply from the boson-fermion model of superconductivity [16]. The low momentum limit of the coefficients  $x_{\vec{p}}$ ,  $y_{\vec{p}}$ ,  $\xi_{\vec{p}}$  and  $\eta_{\vec{p}}$  are all positive and satisfy

$$x_{\vec{p}} - y_{\vec{p}} = s_{\vec{p}}, \quad (5.26)$$

$$x_{\vec{p}} + y_{\vec{p}} = c^2, \quad (5.27)$$

$$\xi_{\vec{p}} - \eta_{\vec{p}} = s'_{\vec{p}} \quad (5.28)$$

and

$$\xi_{\vec{p}} + \eta_{\vec{p}} = \frac{\omega_0^2}{\varrho'_{\vec{p}}} \quad (5.29)$$

with  $s_{\vec{p}}$  and  $s'_{\vec{p}}$  two positive quadratic form of the momentum  $\vec{p}$ . The positivity of  $\eta_{\vec{q}}$  comes from the repulsive nature of the boson-boson interaction and the choice of the condensate phase made in (5.9). The eqs. (5.26) and (5.28) are the consequences of the Goldstone theorem and eq. (5.29) follows from the Coulomb interaction with  $\omega_0$  the plasma frequency. The set of Heisenberg equations of motion read

$$i\dot{\zeta}_{\vec{p}} = x_{\vec{p}}\zeta_{\vec{p}} + y_{\vec{p}}\zeta_{-\vec{p}}^\dagger + \kappa(\beta_{\vec{p}} + \beta_{-\vec{p}}^\dagger), \quad (5.30)$$

$$-i\dot{\zeta}_{-\vec{p}}^\dagger = x_{\vec{p}}\zeta_{-\vec{p}}^\dagger + y_{\vec{p}}\zeta_{\vec{p}} + \kappa(\beta_{\vec{p}} + \beta_{-\vec{p}}^\dagger), \quad (5.31)$$

$$i\dot{\beta}_{\vec{p}} = \xi_{\vec{p}}\beta_{\vec{p}} + \eta_{\vec{p}}\beta_{-\vec{p}}^\dagger + \kappa(\zeta_{\vec{p}} + \zeta_{-\vec{p}}^\dagger), \quad (5.32)$$

$$-i\dot{\beta}_{-\vec{p}}^\dagger = \xi_{\vec{p}}\beta_{-\vec{p}}^\dagger + \eta_{\vec{p}}\beta_{\vec{p}} + \kappa(\zeta_{\vec{p}} + \zeta_{-\vec{p}}^\dagger). \quad (5.33)$$

With the ansatz that  $\zeta_{\vec{p}} \propto e^{-i\Omega t}$ ,  $\zeta_{-\vec{p}} \propto e^{i\Omega t}$ ,  $\beta_{\vec{p}} \propto e^{-i\Omega t}$  and  $\beta_{-\vec{p}} \propto e^{i\Omega t}$ , we obtain the secular equation for the energy  $\Omega$ ,

$$\begin{vmatrix} x_{\vec{p}} - \Omega & y_{\vec{p}} & \kappa & \kappa \\ y_{\vec{p}} & x_{\vec{p}} + \Omega & \kappa & \kappa \\ \kappa & \kappa & \xi_{\vec{p}} - \Omega & \eta_{\vec{p}} \\ \kappa & \kappa & \eta_{\vec{p}} & \xi_{\vec{p}} + \Omega \end{vmatrix} = 0 \quad (5.34)$$

and its solutions:

$$\begin{aligned} \Omega^2 &= \frac{1}{2}[x_{\vec{p}}^2 - y_{\vec{p}}^2 + \xi_{\vec{p}}^2 - \eta_{\vec{p}}^2 \\ &\quad \pm \sqrt{(x_{\vec{p}}^2 - y_{\vec{p}}^2 - \xi_{\vec{p}}^2 + \eta_{\vec{p}}^2)^2 + 4\kappa^2(x_{\vec{p}} - y_{\vec{p}})(\xi_{\vec{p}} - \eta_{\vec{p}})}]. \end{aligned} \quad (5.35)$$

The stability requires that  $E^2 > 0$  which is equivalent to

$$(x_{\vec{p}} + y_{\vec{p}})(\xi_{\vec{p}} + \eta_{\vec{p}}) > \kappa^2 \quad (5.36)$$

and is amply guaranteed by the relations (5.27)-(5.29) for  $\vec{p} \rightarrow 0$ . It follows from (5.26)-(5.29) and (5.35) that the low-lying spectrum is given by

$$E^2 = c^2 \varrho_{\vec{p}} + O(p^4), \quad (5.37)$$

where the  $O(p^4)$  represents the correction from the superconducting order and is therefore rather small.

## 6. Concluding Remarks

We conclude this paper by a few comments related to the real system,  $Sr_2YRu_{1-x}Cu_xO_6$  and  $Ba_2YRu_{1-x}Cu_xO_6$ .

The Monte Carlo simulation and spin wave fitting of the specific data [2] for  $x = 0$  indicates that  $J = 1.28 \sim 2.06$  meV. The closeness of the locations of the two specific heat suggests that we are in the neighborhood of the merging point of the three phases (FM(AF), canting and disorder) and implies  $\frac{b}{JS^2} = 2.5$ , which together with (1.8) gives rise to  $t = 36.0 \sim 57.9$  meV. The large double exchange approximation is therefore quite good for the real system. Assuming only one component of the  $d$ -orbit of  $Ru^{+5}$  gets delocalized, there would be two states per site. Making an equal partition of these delocalized states into four bands, there would be 0.5 states per site and per band. With only one band filled partially, the filling fraction of the band would be  $4x$ . There the low density approximation is not a good one for the observed samples (with  $x=0.07, 0.10$ ). With all three  $d$  components delocalized and degenerate, the filling fraction can be lowered to  $4x/3$  and the accuracy of the low density approximation can be improved.

So far we have concentrated our attention to the magnetic properties of the double exchange system. Now we come to the superconductivity of the system. Since it has not been ruled out that observed superconductivity is caused by the cuprate impurities, we shall list in the following the pros and the cons to a genuine superconductivity of a pure system.

1) Imagine the system  $Sr_2YRu_{1-x}Cu_xO_6$  consists of several domains of pure phases of the double perovskite  $Sr_2YRu_{1-x_n}Cu_{x_n}$  and cuprate  $YSr_2Cu_{3-y_k}Ru_{y_k}O_{7-\delta_m}$ . Suppose that the size of each domain is sufficient large that the interface effect on the stoichiometry may be neglected, we expect that

$$N = \sum_n N_n + \sum_{k,m} N_{k,m}, \quad (6.1)$$

$$N(1-x) = \sum_n N_n(1-x_n) + \sum_{k,m} N_{k,m}y_k, \quad (6.2)$$

$$Nx = \sum_n N_n x_n + \sum_{k,m} N_{k,m} (3 - y_k) \quad (6.3)$$

and so on, where  $N$  is the total number of  $Y$  ion,  $N_n$  is the total number of  $Sr_2YRu_{1-x_n}Cu_{x_n}O_6$  molecules and  $N_{k,m}$  that of  $YSr_2Cu_{3-y_k}Ru_{y_k}O_{7-\delta_m}$  molecules. The eqs (6.1)-(6.3) is the consequence of the balance the numbers of  $Y$ ,  $Sr$ ,  $Ru$  and  $Cu$  ions. Combining (6.2) and (6.3) we find  $N = \sum_n N_n +$

$3 \sum_{k,m} N_{k,m}$ . It follows from (6.1) then that  $N_{k,m} = 0$ , which rules out the bulk impurity phase of cuprates.

2) The coherent length of a cuprate superconductor is comparable to the lattice spacing. A grain with a small number of unit cells of cuprate is already able to sustain a long range order. It may happen that a large number of such grains of cuprates get embedded inside the bulk double perovskite sample. On the other hand, in order to support the bulk resistivity transition, Josephson tunneling between different grains has to be significant. This process, however is made rather difficult by a canting magnetic order since the splitting of the spin degeneracy in the bulk material reduces drastically the tunneling probability of a singlet Cooper pair.

3) If the observed superconductivity is a genuine one coexisting with the canting magnetic order, the pairing is between the itinerant holes with opposite momenta and is of odd parity. The doped  $Cu$ -ions plays the role of impurities, in addition to provide itinerant holes. (In this aspect,  $Sr_2YRu_{1-x}Cu_xO_6$  differs from the cuprates. The doping of the latter does not alter the  $CuO_2$  planes.) These impurities offset the degeneracy between opposite momentum and thereby suppress the superconductivity. This is similar to the effect of magnetic impurities on the singlet pairing. If this factor dominates, the transition temperature would be lowered with doping, opposite to the observation.

Odd parity pairing would be a distinct feature of the superconducting order with canting magnetic order and the parity symmetry is spontaneously broken, i.e.

$$\mathcal{P}|S\rangle \neq |S\rangle, \quad (6.4)$$

where  $\mathcal{P}$  stands for the ordinary inversion operator defined by

$$\mathcal{P}\psi_{\vec{p}}\mathcal{P}^{-1} = \psi_{-\vec{p}}, \quad (6.5)$$

$$\mathcal{P}\zeta_{\vec{p}}\mathcal{P}^{-1} = \zeta_{-\vec{p}}, \quad (6.6)$$

$$\mathcal{P}z_{\vec{p}}\mathcal{P}^{-1} = z_{-\vec{p}} \quad (6.7)$$

and  $\mathcal{P}^2 = 1$ . Unfortunately, such a parity broken does not produce any observational consequence for a homogeneous super phase. A new operator which combines the inversion and a charge rotation through  $\frac{\pi}{2}$ ,

$$\mathcal{P}' = e^{i\frac{\pi}{2}Q}\mathcal{P} \quad (6.6)$$

with  $Q$  the charge operator, leave the condensate invariant. Acting on the observables bilinear in hole operators, momentum, electric current, etc.,  $\mathcal{P}'$  is completely equivalent to  $\mathcal{P}$  since these operators carry no charges. The

square of  $\mathcal{P}'$ , however, assumes different eigenvalues for charge even and charge odd states,  $\mathcal{P}'^2 = (-)^Q$ . But the states with  $Q = \text{even}$  never coher with the states with  $Q = \text{odd}$ , even with a condensate of Cooper pairs of charge  $2e$ .

With both an odd parity superconductor and an even parity superconductor coupled together, none of  $\mathcal{P}$  or  $\mathcal{P}'$  will leave the ground state invariant and observational consequences of the odd parity pairing can be extract.

Furthermore, the pairing state  $|S\rangle$  breaks also the time reversal invariance and this will lead to additional observational effects which may serve as an evidence of a genuine superconductivity.

Another possible way to distinguish a genuine superconductivity from that caused by cuprates is to examine the anisotropicity of the observed superconductivity. X-ray data suggested only moderate anisotropicity of the crystal structure in contrast to the strong anisotropicity of the cuprates because of the quasi-two-dimensional crystal structure.

In addition to the magnetic properties presented in this paper, we have also calculated the usual optical response functions on account of the exotic band structure. The motivation came from the  $\lambda$  term of the Hamiltonian (1.1), which is, with a ferromagnetic order canting order, equivalent to an ultra-strong magnetic field acting on the spin degrees of freedom. The typical Farady angle associated to the optical activity because of  $T$ -violation of the magnetic ordering turns out to be about  $10^{-4}$  radians per wavelength in the visible region and is characterized by a different wavelength dependence from that of the ordinary magneto-optical effect. The details of this work will be reported in a forthcoming publication [17].

## Acknowledgments

Hai-cang Ren is grateful to Professors T. D. Lee and C. S. Ting for discussions. We are indebted to Professors T. K. Lee, C. C. Chi and Dr. D. Y. Chen for valuable conversations. We are also benefitted from Professor Y. S. Wu, Drs. W. E. Jian and C. C. Wu for their participation of the early stage of this work. Part of this work was carried out during Hai-cang Ren's visit in the National Tsing Hua University in 1997 and he would like to thank their hospitality. This work is supported in part by U. S. Department of Energy under Grant DE-FG02-91ER40651, Task B.

## Appendix A

Within the orthorhombic symmetry, we assume that  $\hat{z}$ -axis is the easy axis of the ferromagnetic order and  $\hat{x}$ -axis is the easy axis of the antiferromagnetic order. We add the following anisotropy terms to the effective magnon Hamiltonian (3.36)

$$H'_{\text{mag.}} = H_{\text{mag.}} + \frac{w_+}{S} \sum_{\langle ab \rangle} [\vec{S}_{ab+}^2 - (\vec{S}_{ab+} \cdot \hat{z})^2] + \frac{w_-}{S} \sum_{\langle ab \rangle} [\vec{S}_{ab-}^2 - (\vec{S}_{ab-} \cdot \hat{x})^2], \quad (A.1)$$

where

$$\vec{S}_{ab\pm} = \frac{1}{2}(\vec{S}_a \pm \vec{S}_b) \quad (A.2)$$

and the summation extends to all inter-layer bonds. The new terms leaves  $\mathcal{C}$ -parity intact. Applying the large spin expansions (2.9) and (2.10) with  $\hat{\zeta} = \hat{z}$  and  $\hat{\xi} = \hat{x}$ , and making the Fourier transformations (B.1) and (B.2) below, we find that

$$\begin{aligned} H'_{\text{mag.}} = & \sum_{\vec{q}} x_{\vec{q}}^{\pm\prime} \zeta_{\vec{q}}^\dagger \zeta_{\vec{q}} + \sum_{\vec{q}}' y_{\vec{q}}^{\pm\prime} (\zeta_{\vec{q}} \zeta_{-\vec{q}} + \zeta_{-\vec{q}}^\dagger \zeta_{\vec{q}}^\dagger) \\ & + \sum_{\vec{q}} x_{\vec{q}}^{-\prime} z_{\vec{q}}^\dagger z_{\vec{q}} + \sum_{\vec{q}}' y_{\vec{q}}^{-\prime} (z_{\vec{q}} z_{-\vec{q}} + z_{-\vec{q}}^\dagger z_{\vec{q}}^\dagger), \end{aligned} \quad (A.3)$$

where

$$x_{\vec{q}}^{\pm\prime} = x_{\vec{q}}^\pm + \frac{1}{2} w_+ (4 \mp v_{\vec{q}}) \left( 1 + \cos^2 \frac{\Theta}{2} \right) + \frac{1}{2} w_- (4 \pm v_{\vec{q}}) + \frac{1}{2} (4 \mp v_{\vec{q}}) w_- \sin^2 \frac{\Theta}{2} \quad (A.4)$$

and

$$y_{\vec{q}}^{\pm\prime} = y_{\vec{q}}^\pm - \frac{1}{2} w_+ (4 \mp v_{\vec{q}}) \sin^2 \frac{\Theta}{2} - \frac{1}{2} w_- (4 \pm v_{\vec{q}}) + \frac{1}{2} w_- (4 \mp v_{\vec{q}}) \sin^2 \frac{\Theta}{2} \quad (A.5)$$

with  $x_{\vec{q}}^\pm$  and  $y_{\vec{q}}^\pm$  given in (3.37) and (3.38). Goldstone theorem ceases to hold and energy gaps begin to open between the ground state and the excitations. The energy gap for the magnon of  $\mathcal{C} = 1$  reads

$$\delta_+ = 8\sqrt{2JSw_-} \sin \frac{\Theta}{2} \quad (A.6)$$

and that for the magnon of  $\mathcal{C} = -1$  reads

$$\delta_- = 8\sqrt{w_+ \left( w_+ \cos^2 \frac{\Theta}{2} + w_- \sin^2 \frac{\Theta}{2} \right)}. \quad (A.7)$$

With a fixed canting angle  $\Theta$ , the spin frame can be viewed as the body frame of a rigid rotator and its orientation can be specified by three variables, say

Euler angles. On the other hand, for small vibrations about the laboratory frame (i.e. lattice frame here), the dependence on the precession angle is of higher order in magnitude. This is why only two parameters  $w_{\pm}$  are included in (A.1).

## Appendix B

### 1. Large spin expansion

In this part of the appendix, we shall display the steps which lead from (1.1) to the expressions (2.11)-(2.17). Making Fourier expansion with respect to the lattice Bloch momentum  $\vec{p}$ ,

$$c_a = \sqrt{\frac{2}{N}} \sum_{\vec{p}} c_{\vec{p}} e^{i\vec{p} \cdot \vec{R}_a} \quad (B.1)$$

$$d_b = \sqrt{\frac{2}{N}} \sum_{\vec{p}} d_{\vec{p}} e^{i\vec{p} \cdot \vec{R}_b} \quad (B.2)$$

$$\Psi_a = \sqrt{\frac{2}{N}} \sum_{\vec{p}} \Psi_{\vec{p}}^{(a)} e^{i\vec{p} \cdot \vec{R}_a} \quad (B.3)$$

$$\Psi_b = \sqrt{\frac{2}{N}} \sum_{\vec{p}} \Psi_{\vec{p}}^{(b)} e^{i\vec{p} \cdot \vec{R}_a} \quad (B.4)$$

with  $a$  labeling the sites on  $A$  and  $b$  labeling the sites on  $B$ . Substituting (2.9)-(2.10) and (B.1)-(B.4) into the Hamiltonian (1.1), we obtain

$$H = H_0 + H_1 + H_2 + H_3 + H_4 + U_{Coul.}, \quad (B.5)$$

where

$$H_0 = 2\mathcal{N}S^2(J' + 2J\cos\Theta), \quad (B.6)$$

$$H_1 = 4JS^{\frac{3}{2}}\sqrt{\mathcal{N}}(c_0 + c_0^\dagger - d_0 - d_0^\dagger)\sin\Theta \quad (B.7)$$

$$H_2 = 2J'S \sum_{\vec{p}} (-2 + u_{\vec{p}})(c_{\vec{p}}^\dagger c_{\vec{p}} + d_{\vec{p}}^\dagger d_{\vec{p}})$$

$$+ 2JS \left[ -4 \sum_{\vec{p}} (c_{\vec{p}}^\dagger c_{\vec{p}} + d_{\vec{p}}^\dagger d_{\vec{p}}) \cos\Theta + \sum_{\vec{p}} v_{\vec{p}} (c_{\vec{p}}^\dagger d_{\vec{p}} + d_{\vec{p}}^\dagger c_{\vec{p}}) \cos^2 \frac{\Theta}{2} \right]$$

$$- \sum_{\vec{p}} v_{\vec{p}} (c_{\vec{p}} d_{-\vec{p}} + d_{-\vec{p}}^\dagger c_{\vec{p}}^\dagger) \sin^2 \frac{\Theta}{2} \Big] + \sum_{\vec{p}} \Psi_{\vec{p}}^\dagger (E_{\vec{p}} - \mu) \Psi_{\vec{p}}, \quad (B.8)$$

$$\begin{aligned} H_3 = & \lambda \sqrt{\frac{S}{2\mathcal{N}}} \sum_{\vec{p}, \vec{q}} \left[ c_{\vec{q}} \Psi_{\vec{p} + \frac{\vec{q}}{2}}^\dagger \rho_+ \vec{\tau} \cdot \hat{e}_A^- \Psi_{\vec{p} - \frac{\vec{q}}{2}} + c_{\vec{q}}^\dagger \Psi_{\vec{p} - \frac{\vec{q}}{2}}^\dagger \rho_+ \vec{\tau} \cdot \hat{e}_A^+ \Psi_{\vec{p} + \frac{\vec{q}}{2}} \right. \\ & \left. + d_{\vec{q}} \Psi_{\vec{p} + \frac{\vec{q}}{2}}^\dagger \rho_- \vec{\tau} \cdot \hat{e}_B^- \Psi_{\vec{p} - \frac{\vec{q}}{2}} + d_{\vec{q}}^\dagger \Psi_{\vec{p} - \frac{\vec{q}}{2}}^\dagger \rho_- \vec{\tau} \cdot \hat{e}_B^+ \Psi_{\vec{p} + \frac{\vec{q}}{2}} \right] \\ & + 2J \sqrt{\frac{S}{\mathcal{N}}} \sin \Theta \sum_{\vec{p}, \vec{q}} v_{\vec{q}} \left[ -c_{\vec{q}} d_{\vec{p} + \frac{\vec{q}}{2}}^\dagger d_{\vec{p} - \frac{\vec{q}}{2}} - c_{\vec{q}}^\dagger d_{\vec{p} - \frac{\vec{q}}{2}}^\dagger d_{\vec{p} + \frac{\vec{q}}{2}} \right. \\ & \left. + d_{\vec{q}} c_{\vec{p} + \frac{\vec{q}}{2}}^\dagger c_{\vec{p} - \frac{\vec{q}}{2}} + d_{\vec{q}}^\dagger c_{\vec{p} - \frac{\vec{q}}{2}}^\dagger c_{\vec{p} + \frac{\vec{q}}{2}} \right] \quad (B.9) \end{aligned}$$

$$\begin{aligned} H_4 = & \frac{2J'}{\mathcal{N}} \sum_{\vec{p}, \vec{p}', \vec{q}} u_{\vec{q}} \left( c_{\vec{p}' - \frac{\vec{q}}{2}}^\dagger c_{\vec{p} + \frac{\vec{q}}{2}}^\dagger c_{\vec{p}' + \frac{\vec{q}}{2}} c_{\vec{p} - \frac{\vec{q}}{2}} + d_{\vec{p}' - \frac{\vec{q}}{2}}^\dagger d_{\vec{p} + \frac{\vec{q}}{2}}^\dagger d_{\vec{p}' + \frac{\vec{q}}{2}} d_{\vec{p} - \frac{\vec{q}}{2}} \right) \\ & + \frac{4J}{\mathcal{N}} \cos \Theta \sum_{\vec{p}, \vec{p}', \vec{q}} v_{\vec{q}} c_{\vec{p}' - \frac{\vec{q}}{2}}^\dagger d_{\vec{p} + \frac{\vec{q}}{2}}^\dagger c_{\vec{p}' + \frac{\vec{q}}{2}} d_{\vec{p} - \frac{\vec{q}}{2}} \\ & - \frac{\lambda}{2\mathcal{N}} \sum_{\vec{p}, \vec{p}', \vec{q}} \left( c_{\vec{p}' - \frac{\vec{q}}{2}}^\dagger c_{\vec{p}' + \frac{\vec{q}}{2}} \Psi_{\vec{p} + \frac{\vec{q}}{2}}^\dagger \rho_+ \vec{\tau} \cdot \hat{\zeta}_A \Psi_{\vec{p} - \frac{\vec{q}}{2}} + d_{\vec{p}' - \frac{\vec{q}}{2}}^\dagger d_{\vec{p}' + \frac{\vec{q}}{2}} \Psi_{\vec{p} + \frac{\vec{q}}{2}}^\dagger \rho_- \vec{\tau} \cdot \hat{\zeta}_B \Psi_{\vec{p} - \frac{\vec{q}}{2}} \right). \quad (B.10) \end{aligned}$$

$$\begin{aligned} U_{Coul.} = & \frac{e^2}{\mathcal{N} \varepsilon} \sum_{\vec{p}, \vec{p}', \vec{q}} \left[ D_{\vec{q}}^{(0)} \Psi_{\vec{p} + \frac{\vec{q}}{2}}^\dagger \Psi_{\vec{p}' - \frac{\vec{q}}{2}}^\dagger \Psi_{\vec{p}' + \frac{\vec{q}}{2}} \Psi_{\vec{p} - \frac{\vec{q}}{2}} \right. \\ & \left. + D_{\vec{q}}^{(0)\prime} (\rho_3)_{\alpha\beta} (\rho_3)_{\alpha'\beta'} \Psi_{\vec{p} + \frac{\vec{q}}{2}\alpha}^\dagger \Psi_{\vec{p}' - \frac{\vec{q}}{2}\alpha'}^\dagger \Psi_{\vec{p}' + \frac{\vec{q}}{2}\beta'} \Psi_{\vec{p} - \frac{\vec{q}}{2}\beta} \right], \quad (B.11) \end{aligned}$$

In the above expansion, we have combined hole operators  $\Psi_{\vec{p}}^{(a)}$  and  $\Psi_{\vec{p}}^{(b)}$ , each of two components, into a  $4 \times 1$  column matrix,

$$\Psi_{\vec{p}} = \begin{pmatrix} \Psi_{\vec{p}}^{(a)} \\ \Psi_{\vec{p}}^{(b)} \end{pmatrix}. \quad (B.12)$$

Accordingly,  $\tau$ 's and  $\rho$ 's stand for the  $4 \times 4$  Dirac matrices (2.18)-(2.19) with  $\vec{\tau} = \tau_1 \hat{\xi} + \tau_2 \hat{\eta} + \tau_3 \hat{\zeta}$  and  $\rho_{\pm} = \frac{1 \pm \rho_3}{2}$ . The  $4 \times 4$  matrix  $E_{\vec{p}}$  is given by

$$E_{\vec{p}} = -t' u_{\vec{p}} - t v_{\vec{p}} \rho_1 + \frac{1}{2} \lambda S (\rho_+ \hat{\zeta}_A \cdot \vec{\tau} + \rho_- \hat{\zeta}_B \cdot \vec{\tau}) \quad (B.13)$$

and the unit vectors  $\hat{e}_{A(B)}^\pm$  is defined as

$$\hat{e}_A^\pm = \frac{1}{\sqrt{2}}(\hat{\xi}_A \pm i\hat{\eta}) \quad (B.14)$$

and

$$\hat{e}_B^\pm = \frac{1}{\sqrt{2}}(\hat{\xi}_B \pm i\hat{\eta}). \quad (B.15)$$

$u_{\vec{p}}$  and  $v_{\vec{p}}$  in the above equations are given by (2.25) and (2.26)

In addition to invariance under the tetragonal crystal rotation, inversion, the following transformation  $\mathcal{C}$ ,

$$\mathcal{C}c_{\vec{p}}\mathcal{C}^{-1} = -d_{\vec{p}}, \quad (B.16)$$

$$\mathcal{C}d_{\vec{p}}\mathcal{C}^{-1} = -c_{\vec{p}} \quad (B.17)$$

and

$$\mathcal{C}\Psi_{\vec{p}}\mathcal{C}^{-1} = C\Psi_{\vec{p}} \quad (B.18)$$

with  $C = -i\rho_1 e^{-\frac{i\pi}{2}\tau_3} = -\rho_1\tau_3$  also leaves the Hamiltonian (B.5)-(B.11) unchanged. This transformation amounts to interchange the sublattices  $A$  and  $B$  while making a  $\pi$  rotation of the ion spins about  $z$ -axis. The time reversal invariance is broken by the magnetic ordering. This symmetry can be diagonalized via the following unitary transformation:

$$c_{\vec{p}} = \frac{1}{\sqrt{2}}(z_{\vec{p}} + \zeta_{\vec{p}}), \quad (B.19)$$

$$d_{\vec{p}} = \frac{1}{\sqrt{2}}(z_{\vec{p}} - \zeta_{\vec{p}}), \quad (B.20)$$

$$\Psi_{\vec{p}} = V\psi_{\vec{p}}, \quad (B.21)$$

where

$$V = \frac{1}{\sqrt{2}}(\rho_- + \rho_+\tau_3)(\rho_1 + \rho_3)\left(\cos\frac{\Theta}{4} - i\tau_2\sin\frac{\Theta}{4}\right). \quad (B.22)$$

In terms these new operators, the transformation laws (2.29)-(2.31) follow and a simpler form of the Hamiltonian, (2.11)-(2.17), emerges.

### B.2, Coulomb vertex

In what follows, we shall calculate the Coulomb vertex. Labeling the sites on the sublattice  $a$  and those on the sublattice by  $b$ , we have

$$U_{Coul.} = \frac{e^2}{8\pi\varepsilon} \left[ U \left( \sum_a : \varrho_a \varrho_a : + \sum_b : \varrho_b \varrho_b : \right) \right]$$

$$+ \sum_{a \neq a'} \frac{:\varrho_a \varrho_{a'}:}{|\vec{R}_a - \vec{R}_{a'}|} + \sum_{b \neq b'} \frac{:\varrho_b \varrho_{b'}:}{|\vec{R}_b - \vec{R}_{b'}|} + 2 \sum_{ab} \frac{:\varrho_a \varrho_b:}{|\vec{R}_a - \vec{R}_b|} \Big], \quad (B.23)$$

where

$$\varrho_j = \Psi_j^\dagger \Psi_j, \quad (B.24)$$

with  $j = a, b$  and  $:(\dots):$  denotes the normal ordering. Making the Fourier transformation in (B.3)-(B.4), we obtain

$$U_{Coul.} = \frac{e^2}{2\mathcal{N}\varepsilon} \left[ \sum_{\vec{q}} (S_{\vec{q}} + S'_{\vec{q}}) : \varrho_{-\vec{q}} \varrho_{\vec{q}} : + \sum_{\vec{q}} (S_{\vec{q}} - S'_{\vec{q}}) : \varrho'_{-\vec{q}} \varrho'_{\vec{q}} : \right], \quad (B.25)$$

where

$$\varrho_{\vec{q}} = \sum_{\vec{p}} \Psi_{\vec{p}+\frac{\vec{q}}{2}}^\dagger \Psi_{\vec{p}-\frac{\vec{q}}{2}} = \sum_{\vec{p}} \psi_{\vec{p}+\frac{\vec{q}}{2}}^\dagger \psi_{\vec{p}-\frac{\vec{q}}{2}} \quad (B.26)$$

and

$$\varrho'_{\vec{q}} = \sum_{\vec{p}} \Psi_{\vec{p}+\frac{\vec{q}}{2}}^\dagger \rho_3 \Psi_{\vec{p}-\frac{\vec{q}}{2}} = \sum_{\vec{p}} \psi_{\vec{p}+\frac{\vec{q}}{2}}^\dagger \rho_1 \psi_{\vec{p}-\frac{\vec{q}}{2}} \quad (B.27)$$

with  $\Psi_{\vec{p}}$  and  $\psi_{\vec{p}}$  related by the transformation (B.21).  $S_{\vec{q}}$  and  $S'_{\vec{q}}$  denote two Madelung type sums,

$$S_{\vec{q}} = U + \frac{1}{4\pi} \sum_{\vec{n} \neq 0} \frac{e^{-i\vec{q} \cdot \vec{R}_n}}{R_n} \quad (B.28)$$

and

$$S'_{\vec{q}} = \frac{1}{4\pi} \sum_{\vec{n}} \frac{e^{-i\vec{q} \cdot \vec{R}'_n}}{R'_n} \quad (B.29)$$

with

$$\vec{R}_n = \frac{l}{2} [n_1(\hat{x} + \hat{y}) + n_2(-\hat{x} + \hat{y})] + n_3 l \hat{z} \quad (B.30)$$

and

$$\vec{R}'_n = \frac{l}{2} \left[ \left( n_1 + \frac{1}{2} \right) (\hat{x} + \hat{y}) + \left( n_2 + \frac{1}{2} \right) (-\hat{x} + \hat{y}) \right] + \left( n_3 + \frac{1}{2} \right) l \hat{z} \quad (B.31).$$

It follows that  $\varrho_{\vec{q}}^+$  is  $\mathcal{C}$  even and  $\varrho_{\vec{q}}^-$  is  $\mathcal{C}$  odd. The whole Coulomb energy is therefore invariant under  $\mathcal{C}$ , but both branches of the magnons couple to the Coulomb interaction.  $D_{\vec{q}}^{(0)}$  and  $D_{\vec{q}}^{(0')}$  in the text is given by

$$D_{\vec{q}}^{(0)} = S_{\vec{q}} + S'_{\vec{q}} \quad (B.32)$$

and

$$D_{\vec{q}}^{(0)\prime} = S_{\vec{q}} + S'_{\vec{q}} \quad (B.33)$$

The calculations of  $D_{\vec{q}}^{(0)}$  and  $D_{\vec{q}}^{(0)\prime}$  at low  $\vec{q}$  are similar and we illustrate the method by  $D_{\vec{q}}^{(0)}$ . We first exponentiate the denominator of the summand of (B.28).

$$\frac{1}{R_n} = \frac{\sqrt{2}}{l} \int_0^\infty dt t^{-\frac{1}{2}} e^{-\pi t(n_1^2 + n_2^2 + 2n_3^3)} \quad (B.34)$$

and interchange the order of the integration and the summation, i.e.

$$S_{\vec{q}} = U + \frac{\sqrt{2}}{4\pi l} \int_0^\infty dt t^{-\frac{1}{2}} \left[ \vartheta_3\left(\frac{\alpha_1}{2}|it\right) \vartheta_3\left(\frac{\alpha_2}{2}|it\right) \vartheta_3\left(\frac{\alpha_3}{2}|2it\right) - 1 \right], \quad (B.35)$$

where

$$\vartheta_3(z|\tau) = 1 + 2 \sum_{n=1}^{\infty} e^{in^2\pi\tau} \cos 2nz \quad (B.36)$$

is one of Jacobian theta function [18]. Using the formula

$$\vartheta_3(z|\tau) = (-i\tau)^{-\frac{1}{2}} \exp\left(\frac{z^2}{i\pi\tau}\right) \vartheta_3\left(\frac{z}{\tau} \mid -\frac{1}{\tau}\right), \quad (B.37)$$

we have

$$S_{\vec{q}} = U + \frac{1}{4\pi l} \int_0^\infty dt t^{-\frac{1}{2}} \left[ -\sqrt{2} + t^{-\frac{3}{2}} e^{-\frac{2\alpha_\perp^2 + \alpha_3^2}{8\pi t}} \vartheta_3\left(-i\frac{\alpha_1}{2t} \mid \frac{i}{t}\right) \vartheta_3\left(-i\frac{\alpha_2}{2t} \mid \frac{i}{t}\right) \vartheta_3\left(-i\frac{\alpha_3}{4t} \mid \frac{i}{2t}\right) \right]. \quad (B.38)$$

Only the "1" term of each  $\vartheta_3$  factor of (B.38) is sensitive to the limit  $\vec{q} \rightarrow 0$  upon integration. By isolating out this term and setting  $\vec{q} = 0$  for the rest, we arrive at

$$S_{\vec{q}} = U + \frac{2}{l(2\alpha_\perp^2 + \alpha_3^2)} + C, \quad (B.39)$$

where

$$C = \frac{1}{4\pi l} \int_0^\infty \left[ t^{-2} \left[ \vartheta_3^2\left(0 \mid \frac{i}{t}\right) \vartheta_3\left(0 \mid \frac{i}{2t}\right) - 1 \right] - \sqrt{\frac{2}{t}} \right] = -\frac{0.27214}{l}. \quad (B.40)$$

Likewise we obtain that

$$S_{\vec{q}}^{(0)\prime} = \frac{2}{l(2\alpha_\perp^2 + \alpha_3^2)} - \frac{0.092711}{l}. \quad (B.41)$$

Substituting (B.39) and (B.41) into (B.32) and (B.33), we end up with (2.27) and (2.28). Only the magnon of  $\mathcal{C} = 1$  couple to the long range tail of the Coulomb force.

## Appendix C

In this appendix, we calculate the decay rate of the magnon with  $\mathcal{C} = 1$ . Neglecting possible couplings to the superconducting order, the effective magnon Hamiltonian for  $\mathcal{C} = 1$  corresponds to the first two terms of () with

$$x_{\vec{p}} = \nu_{\vec{p}}^+ + \Pi_+(0, \vec{p}) \quad (C.1)$$

and

$$y_{\vec{p}} = \Lambda_+(0, \vec{p}). \quad (C.2)$$

A mass-shell magnon operator is given by the following Bogoliubov transformation:

$$\begin{aligned} \gamma_{\vec{p}} &= \zeta_{\vec{p}} \cosh \chi_{\vec{p}} + \zeta_{-\vec{p}}^\dagger \sinh \chi_{\vec{p}}, \\ \gamma_{-\vec{p}}^\dagger &= \zeta_{\vec{p}} \sinh \chi_{\vec{p}} + \zeta_{-\vec{p}}^\dagger \cosh \chi_{\vec{p}} \end{aligned} \quad (C.3)$$

where

$$\cosh \chi_{\vec{p}} = \frac{x_{\vec{p}}}{\omega_{\vec{p}}^+}$$

,

$$\sinh \chi_{\vec{p}} = \frac{y_{\vec{p}}}{\omega_{\vec{p}}^+}$$

with  $\omega_{\vec{p}}^+ = \sqrt{x_{\vec{p}}^2 - y_{\vec{p}}^2}$ , whose low momentum limit is given explicitly in (3.32). The amplitude for a magnon with momentum  $\vec{q}$  to decay into a pair of an electron and a hole with momenta  $\vec{p} \pm \frac{\vec{q}}{2}$  near the Fermi surface,  $\mathcal{A}_{\vec{p}, \vec{q}}$ , corresponds to the superposition of the two sets of diagrams in Fig. 9, i. e.

$$\mathcal{A}_{\vec{p}, \vec{q}} = \mathcal{U}_{\vec{p} + \frac{\vec{q}}{2}}^{+\dagger} \left( (\text{Fig.9a}) \cosh \chi_{\vec{q}} - (\text{Fig.9b}) \sinh \chi_{\vec{q}} \right) \mathcal{U}_{\vec{p} - \frac{\vec{q}}{2}+}^+. \quad (C.4)$$

With the aid of the Feynman rules listed in the section 3, we find that

$$\begin{aligned} \mathcal{A}_{\vec{p}, \vec{q}} &= i\lambda \sqrt{\frac{S}{2N}} \phi_{\vec{p} + \frac{\vec{q}}{2}+}^{+\dagger} \left[ \sigma_- \cosh \chi_{\vec{q}} - \sigma_+ \sinh \chi_{\vec{q}} \right. \\ &\quad \left. + 2 \frac{D_{\vec{q}}^{(0)}}{\varepsilon + D_{\vec{q}}^{(0)} \sigma(\omega, \vec{q})} \frac{t}{\lambda S} \sin \frac{\Theta}{2} [C(\omega, \vec{q}) \cosh \chi_{\vec{q}} - C(-\omega, -\vec{q}) \sinh \chi_{\vec{q}}] \right] \phi_{\vec{p} - \frac{\vec{q}}{2}+}^+, \end{aligned} \quad (C.5)$$

where the functions  $D_{\vec{q}}^{(0)}$ ,  $\sigma(\omega, \vec{q})$  and  $C(\omega, \vec{q})$  are defined in section 3 with  $\omega = \omega_{\vec{q}}^+$ .

Following the same reasoning employed in section 3, we approximate  $C(\omega, \vec{q})$  and  $\sigma(\omega, \vec{q})$  by  $C(0, \vec{q})$  and  $\sigma(0, \vec{q})$  and obtain, after some algebra

$$|\mathcal{A}_{\vec{p}, \vec{q}}|^2 = \frac{t^2}{2\mathcal{N}S} \left[ \frac{1}{2} (v_{\vec{p}+\frac{\vec{q}}{2}} - v_{\vec{p}-\frac{\vec{q}}{2}})^2 \cosh 2\chi_{\vec{q}} - (v_{\vec{p}} - \langle v \rangle) (v_{\vec{p}+\frac{\vec{q}}{2}} - v_{\vec{p}-\frac{\vec{q}}{2}}) \right. \\ \left. + (v_{\vec{p}} - \langle v \rangle)^2 (\cosh \chi_{\vec{q}} - \sinh \chi_{\vec{q}})^2 \right] \sin^2 \frac{\Theta}{2} \quad (C.6)$$

for small  $\vec{q}$ , where  $\langle \dots \rangle$  denotes the same Fermi surface average defined in (3.30). The decay width is given by

$$\Gamma_{\vec{q}} = 2\pi \sum_{\vec{p}} |\mathcal{A}_{\vec{p}, \vec{q}}|^2 \theta(\epsilon_{\vec{p}+\frac{\vec{q}}{2}}) \theta(-\epsilon_{\vec{p}-\frac{\vec{q}}{2}}) \delta(\epsilon_{\vec{p}+\frac{\vec{q}}{2}} - \epsilon_{\vec{p}-\frac{\vec{q}}{2}} - \omega_{\vec{q}}^+). \quad (C.7)$$

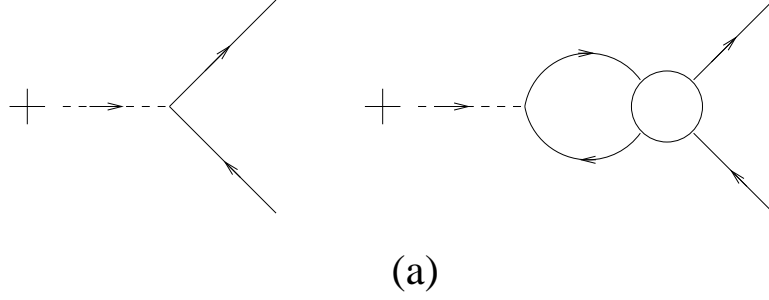
With parabolic approximation of  $u_{\vec{p}}$  and  $v_{\vec{p}}$  and low carrier density,  $n_h \ll 1$ ,  $p^2$  is of the order of  $n_h^{\frac{2}{3}}$  so is the Fermi energy measured from the bottom of the conducting band,  $\epsilon_F = \mu + 2t' + 4t \cos \frac{\Theta}{2}$ . The order of the first term of (C.6) is  $n_h^{\frac{2}{3}}$ , the order of the second term is  $n_h$  and that of the third term is  $n_h^{\frac{4}{3}}$ . Keeping only the first term of  $|\mathcal{A}_{\vec{p}, \vec{q}}|^2$  and completing the phase space integral for small  $\vec{q}$ , we obtain

$$\Gamma_{\vec{q}} = \frac{2}{\pi S} \frac{JS t'^2 \epsilon_F \alpha \sin^2 \beta \cos^2 \beta}{(t' + t \cos \frac{\Theta}{2})^2 (t' \sin^2 \beta + t \cos \frac{\Theta}{2})^{\frac{3}{2}} \sqrt{t \cos \frac{\Theta}{2}}} \tan \frac{\Theta}{2} \sin^3 \frac{\Theta}{2}, \quad (C.8)$$

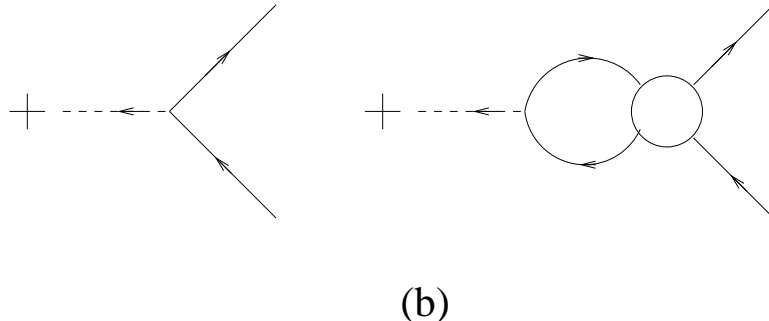
where we have parametrized the magnon energy  $\omega_{\vec{q}}^+$  by  $\omega_{\vec{q}}^+ = c\alpha \sin \beta$  with  $\alpha = \sqrt{\alpha_1^2 + \alpha_2^2 + \alpha_3^2}$  and  $\sin \beta = \alpha_{\perp}/\alpha$ . The contribution from the second term in the bracket of (C.6) has been neglected in (C.8) since it is of higher power of the hole density,  $n_h$ , when  $n_h \ll 1$ . As far as the order of magnitude concerned, we have  $c \sim JS$ ,  $t' \sim t$ , and  $JS^2 \sim tn$ . It follows then that

$$\frac{\Gamma_{\vec{q}}}{\omega_{\vec{q}}^+} \sim \frac{1}{S} n_h^{\frac{2}{3}} \ll 1 \quad (C.9)$$

for large spin and small carrier density.



(a)



(b)

Figure 9 The Feynman diagrams for the decay of a magnon with  $\mathcal{C} = 1$ . The open circle with four legs stands for the dressed Coulomb vertex as in Fig. 4.

## REFERENCES

1. M. K. Wu, et. al., *Z. Phys.*, **102**, 37 (1997).
2. M. K. Wu, et. al., submitted to *Phys. Rev. Lett.*.
3. C. Zener, *Phys. Rev.*, **82**, 403 (1951).
4. P. W. Anderson and H. Hasegawa, *Phys. Rev.*, **100**, 675 (1955).
5. P. G. de Gennes, *Phys. Rev.* **118**, 141 (1960).
6. A. J. Millis, P. B. Littlewood and B. I. Shraiman, *Phys. Rev. Lett.*, **74**, 5144 (1995).
7. P. D. Battle and W. I. J. Macklin, *J. Solid State Chem.*, **52**, 138 (1984).
8. T. Holstein and H. Primakoff, *Phys. Rev.* **58**, 1098 (1940).
9. N. M. Hugenholtz and D. Pines, *Phys. Rev.* **116**, 489 (1959).
10. M. Creutz, 'Quarks, Gluons and Lattices', Cambridge University Press, 1983.
11. To avoid cumbersome expressions, we have suppressed the infinitesimal imaginary part of the denominators of  $\Pi_+^{(0)}(q_0, \vec{q})$ ,  $\Lambda_+^{(0)}(q_0, \vec{q})$ ,  $C(q_0, \vec{q})$  and  $\sigma(q_0, \vec{q})$  and supplemented with an equivalent rule that the imaginary parts of these functions for real  $q_0$  has to be negative, as is evident from Dyson-Wick perturbation theory.
12. A. J. Leggett, *Rev. Mod. Phys.*, **43**, 331 (1975).
13. See for example, A. L. Fetter and J. D. Walecka, 'Quantum Theory of Many Particle System', Chapter 12, (McGrawHill, New York, 1971).

14. W. E. Pickett, Phys. Rev. Lett., **77**, 3185 (1996).
15. Rigorously speaking, pairing term in the Hamiltonian (5.6) violates the tetragonal symmetry of the original Hamiltonian (1.1). On the other hand, the Goldstone theorem can be verified to the leading order of the low carrier density. A rigorous treatment of the pairing effect should respect the original symmetry and therefore should be extended to all bands.
16. R. Friedberg, T. D. Lee and H. C. Ren, Phys. Rev. **B42**, 4122 (1990).
17. H. C. Ren and M. K. Wu, in preparation.
18. E. T. Whittaker and G. N. Watson, 'A Course of Modern Analysis', 4th ed., Chapter XXI, Cambridge University Press, 1927.